ISSN 2096-7071 (Print)
ISSN 2097-3101 (Online)
CN 10-1629/R1

CHINA CDC WEEKLY

Vol. 8 No. 14 Apr. 3, 2026

中国疾病预防控制中心周报(英文)

Preplanned Studies

Perspectives

ISSN 2096-7071

China CDC Weekly

Editorial Board

Editorial Office

Cover Image: adapted from the World Health Organization, https://www.who.int/campaigns/world-health-day/2026.

Preplanned Studies

Health Risk Assessment of the Large-Scale Heat Waves — Northern China, 2023

Chen Chen[1]; Runmei Ma[1]; Shunshun Zhang[2]; Yueqiao Zhou[1]; Wenfeng Fan[1]; Haiqiong Lu[1]; Yuanyuan Liu[1]; Qing Wang[1]; Tiantian Li[1,#]

Summary

What is already known about this topic?

Heat waves pose significant mortality risks, particularly for older persons and those with cardiovascular diseases, as established in studies in the United States and China.

What is added by this report?

This report quantifies the impact of the unprecedented June 2023 heat waves in Northern China across 420 counties, documenting 599 early-onset, intense, prolonged events and estimating excess mortality at 6.1 per million overall (higher at 4.7 for thoses agaed over 65 years and 5.6 for cardiovascular patients), including 6.2 per million from one prolonged June 21 to 27 wave.

What are the implications for public health practice?

Findings support implementing targeted early warning systems and protective interventions for vulnerable groups like old adults and cardiovascular patients during similar extreme heat events.

ABSTRACT

Introduction: In the summer of 2023, the world experienced unprecedented heat waves that broke previous records. As a typical sensitive area affected by global climate change, northern China is one of the most severely impacted regions.

Methods: This study used heat wave health risk assessment technology to estimate excess deaths from heat waves occurring in 420 counties in northern China in June 2023. We used 24-hour daily mean temperatures as an assessment indicator of heat wave exposure, which were derived from the National Meteorological Science Data Center. Demographic data were obtained from the Seventh National Population Census of China in 2020. Population mortality data were collected from the 2020 China Death Surveillance Dataset. Parameters from a time-series study on heat wave mortality risks across 272 Chinese cities were used to calculate the exposure-response relationship.

Results: In June 2023, 420 counties of northern China experienced a total of 599 heat waves, characterized by early onset, extreme heat intensity, long duration, and widespread impact. Heat wave-attributable excess mortality risk was 6.1 per million people, with the older persons aged ≥65 (4.7 per million people) and patients with cardiovascular diseases (5.6 per million people) more severely affected.

Conclusion: The June 2023 heat wave in northern China threatened the health of residents, especially the older persons and patients with cardiovascular diseases. These findings support the use of targeted warning systems and interventions to protect vulnerable populations in similar situations.

In the summer of 2023, the world experienced unprecedented heat waves that broke previous records (*1*). The global near-surface average temperature in 2023 was 1.45±0.12 °C higher than the average temperature from 1850 to 1900, breaking the previous record of the hottest years, 2016 and 2022, and the summer heat wave affected several regions of the northern Hemisphere (*1*). As a region typically sensitive to global climate change, northern China is one of the most affected areas because of its numerous densely populated large cities. In June 2023 alone, northern China suffered a record-breaking large-scale heat wave, with the average maximum temperature hitting a historical peak of the highest temperature since 1961. The temperature at 124 national meteorological stations exceeded 40 °C, of which 26 stations exceeded the historical extreme value (*2*), ranking first in China's regional high temperature process over the past 33 years, which attracted great attention from the government, media, and the public.

To assess the health impacts associated with the June

2023 heat wave in northern China, we conducted a heat wave health risk assessment covering 420 counties across 36 cities in northern China (Supplementary Table S1, available at https://weekly.chinacdc.cn/). Referring to the commonly used definitions of heat waves in climate change health studies (*3*–*4*), we defined a heat wave as an event in which the average daily temperature exceeds the 97.5th percentile of the historical baseline and lasts for two or more days. Using the average daily temperature from 2013 to 2020 as a historical baseline, we assessed the heat wave exposure characteristics of residents in the region and the excess mortality risk of the population in June 2023, and identified vulnerable populations and high-risk areas. Our findings can provide scientific evidence for the development of health protection measures and strategies for coping with heat waves in the future.

To assess the exposure and health risks of heat waves over northern China from June 1 to June 30, 2023, we obtained 24-hour daily mean temperatures for 420 counties across 36 cities from the National Meteorological Science Data Center. When calculating the exposure-response relationship, the parameters were derived from a time-series study of heat wave mortality risks in 272 Chinese cities (*4*). Demographic data were obtained from the Seventh National Population Census of China in 2020, implemented by the National Bureau of Statistics of China. Population mortality data were collected from the Cause-of-Death Surveillance dataset of the National Cause-of-Death Surveillance System in 2020. The data cover annual mortality rates for nonaccidental, circulatory, and respiratory diseases in the total population, as well as mortality rates for males, females, and individuals aged 65 and above.

We quantified the mortality risk of local heat wave-affected populations in June 2023 using counties as the unit of assessment to calculate the number of excess heat wave-related deaths in each of the 420 counties using Equation (1). We then calculated the excess deaths associated with heat wave exposure in each city using Equation (2), followed by summation to estimate the total number of heat wave-related excess deaths in northern China. We also used Equation (3) to calculate the number of excess deaths due to heat waves per million people on a city scale, known as the excess mortality rate (*EMR*). We performed sensitivity analyses using region-specific exposure-response coefficients for the Temperate Monsoon Zone derived from the same study of 272 Chinese cities (*4*).

$$M_{ij} = \left(RR_{ij} - 1\right) / RR_{ij} \times POP_i \times Y_{ij} \times L_i \quad (1)$$

$$M_j = \sum_{i=1}^{n} M_{ij} \quad (2)$$

$$EMR = M_j / POP_i \times 1000000 \quad (3)$$

In these formulas, M_{ij} represents the number of heat wave-related excess deaths from a specific cause j in county i in June 2023. M_j represents the total excess deaths from a specific cause j associated with heat wave exposure in a given city. RR_{ij} refers to the relative risk of specific-cause death j related to heat waves in the county. POP_i represents the permanent resident population/subpopulation of the assessment area in county i. Y_{ij} is the daily mortality rate for a specific cause of death j in county i. L_i refers to the number of heat wave exposure days in county i in June 2023, and n indicates the number of counties in a particular city. *EMR* denotes the number of excess deaths per million people due to heat wave exposure at the city scale. The R Statistical software (version 4.0.2; Kurt Hornik and R Core Team, Vienna, Austria) was used to perform all analyses.

Table 1 shows the summary statistics of heat wave exposure and heat wave intensity in 420 counties in northern China in June 2023. During the study period, 599 heat waves occurred across the 420 counties. Compared with the same period in previous years, the heat wave in June 2023 exhibited four typical characteristics: early onset, wide impact, high heat intensity, and long duration. As early as June 14, a large-scale heat wave occurred, affecting 37 counties in Beijing, Hebei, Shaanxi, and Inner Mongolia provincial-level administrative divisions (PLADs). Throughout June 2023, 334 counties experienced heat waves, accounting for 79.5% of the total number of counties. A total of 225 counties in Beijing, Tianjin, central Inner Mongolia, and most of Hebei Province have experienced two or more heat waves. Eighty-three counties in Beijing, Tianjin, central Hebei Province, and southeastern Inner Mongolia had daily maximum temperatures exceeding 40 °C three times or more, and 34 of those counties had daily maximum temperatures exceeding 40 °C five times or more. In terms of duration, 133 counties in Beijing, Tianjin, central Inner Mongolia, and most of Hebei Province experienced heat waves lasting four days or more. After June 21, heat waves in Chifeng City and the Xilin Gol League in Inner Mongolia PLAD lasted for six days.

Figure 1 shows the results of the heat wave population health risk assessment and the spatial

TABLE 1. Summary statistics of heat wave exposure in 420 counties of northern China, June 2023.

Region	Frequency of heat waves	Number of heat wave days	Number of heat wave days per county	Number of counties exposed to ≥1 heat wave (proportion %)	Number of counties exposed to ≥2 heat waves (proportion %)	Number of counties exposed to extreme heat* for ≥3 days (proportion %)	Number of counties exposed to extreme heat* for ≥5 days (proportion %)
420 counties	599	1,803	4	334 (79.5)	225 (53.6)	83 (19.8)	34 (8.1)
Inner Mongolia	138	426	4	89 (86.4)	49 (47.6)	0 (0)	0 (0.0)
Beijing	38	133	8	16 (100.0)	16 (100.0)	13 (81.3)	5 (31.3)
Tianjin	32	97	6	16 (100.0)	16 (100.0)	13 (81.3)	1 (6.3)
Shanxi	62	165	1	49 (41.9)	13 (11.1)	0 (0)	0 (0.0)
Hebei	329	982	5	164 (97.6)	131 (78.0)	57 (33.9)	28 (16.7)

Note: * Extreme heat refers to a daily maximum temperature ≥40 ℃.

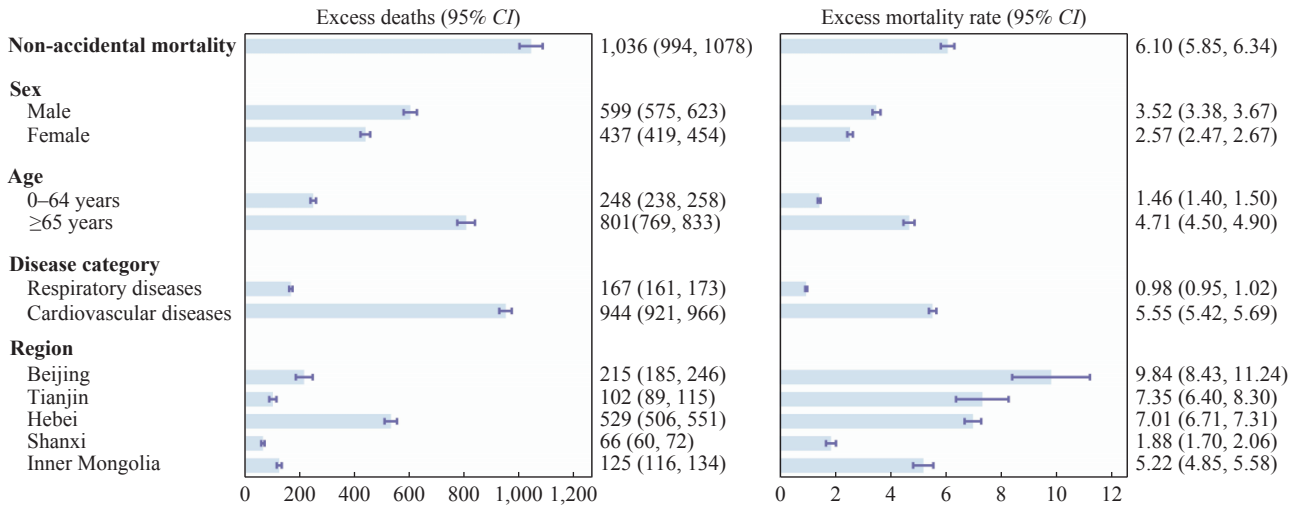

FIGURE 1. Excess deaths and excess mortality rate due to heat waves in 420 counties of northern China in June 2023. Abbreviation: *CI*=confidence interval.

distribution of the excess mortality risk from nonaccidental diseases attributable to heat waves across the five provinces/municipalities. Heat waves resulted in 1,036 excess deaths. High-risk areas are concentrated in Beijing (9.84 per million people), Tianjin (7.35 per million people), Hebei Province (7.01 per million people), and Inner Mongolia (5.22 per million people) PLAD. Older persons and patients with cardiovascular diseases are at high risk of heat waves. Moreover, heat waves with longer duration, greater intensity, and wider coverage exert more severe health impacts. Between June 21 and 27, a large-scale extreme heat wave occurred, affecting 332 counties in 32 cities, with an estimated 614 excess deaths, accounting for 59.2% of the excess deaths from nonaccidental diseases caused by the heat wave that month. Baoding and Chengde of Hebei Province experienced a heat wave that lasted for five consecutive days from June 21 to 25, whereas Chifeng and Xilin Gol League of Inner Mongolia experienced a heat wave that lasted for six days from June 22 to 27. These heat waves across the four cities affected a total of 1.82 million people in 7 counties, and the estimated excess mortality risk attributable to the heat wave was 6.2 per million people.

Supplementary Table S2 (available at https://weekly.chinacdc.cn/) presents the sensitivity analysis of excess deaths from nonaccidental diseases estimated using the exposure-response parameters for the Temperate Monsoon Zone. Given that the relative risk for this climate zone was comparable to the national average, the estimated number of excess deaths derived from region-specific parameters showed no statistically significant difference from the main analysis, while exhibiting wider confidence intervals.

DISCUSSION

The first heat wave in northern China in June 2023 had the characteristics of early onset, long duration, and large scale and the risk was more prominent. The risk of death from the first heat wave was significantly higher than that from subsequent heat waves (*5*–*6*). A study of 43 communities in the United States found a 5.04% increase in all-cause mortality during the first heat wave and a 2.65% increase in subsequent heat waves compared with non-heat wave days (*5*). A study of 130 counties in China also showed that the first heat wave increased the overall risk of death by 16.3% and the risk of cardiovascular death by 23.8% (*6*). This may be because when the first heat wave arrives, the human body has not yet formed a heat adaptation mechanism, including the failure of body temperature regulation functions (such as vasodilation and sweating to respond in time) and people's behavior to adapt to heat lags (such as not increasing the use of air conditioning and not reducing outdoor activities). Since the national average exposure-response relationship parameter was used in this assessment, the actual risk of death from the first heat wave is likely to be even higher than that reported in our results; therefore, the health hazards of the June 2023 heat wave in northern China should be treated seriously.

The older population and patients with cardiovascular diseases are at high risk of exposure to large-scale heat waves (*7*–*9*). Older persons are at a higher risk of dying from heat waves, and the mechanisms include the deterioration of thermoregulatory function due to aging, underlying medical conditions, and long-term use of drugs that impair heat adaptation, as well as delayed access to cooling facilities and untimely medical care due to economic or mobility restrictions (*7*). For patients with cardiovascular disease, Chaseling et al. (*9*) demonstrated that heat waves can cause skin vasodilation (resulting in increased cardiac output) and dehydration (leading to increased blood viscosity), both of which together increase the heart workload. Heat waves can also induce systemic inflammatory responses, promote thrombosis, and exacerbate acute cardiovascular events. We recommend that older people and those with cardiovascular diseases should be included in the core population for heat wave protection, and risk interventions and health protection should be implemented early in the summer to reduce their health risks.

To effectively respond to heat waves, the National Bureau of Disease Control and Prevention issued the Guidelines for Public Health Protection of Heat Waves to guide the public to take scientific precautions, and the health department has implemented multichannel science popularization and education to enhance public awareness and prevention of heat health risks. To address the growing health threat of heat waves under global warming trends, there is an urgent need for action to strengthen heat wave resilience, reduce the risk of death, and prevent the onset of allergies, especially for early warnings and timely responses to such early onset, long-duration, and large-scale heat waves. We recommend strengthening the capacity of disease control agencies for the early warning of thermal health risks. Therefore, population health risk assessment mechanisms should be further improved to consolidate the foundation of risk management. Simultaneously, a normalized popular science education system should be established to continuously enhance the public awareness of protection.

This study has several limitations. First, national-level parameters were selected to ensure statistical stability, as the source dataset already encompassed the study region. While potentially overlooking regional heterogeneity, sensitivity analyses confirmed that region-specific estimates were consistent with the main results, but had wider confidence intervals due to smaller sample sizes; thus, our estimates serve as robust approximations. Second, we estimated excess deaths based on the 97.5th percentile definition (≥2 days) because coefficients for alternative definitions (e.g., 95th, 99th) were either unavailable or statistically insignificant in the source study. While enabling a comprehensive subgroup assessment, this limits its applicability to other definitions, warranting future research on varying heat wave characteristics. Finally, as a rapid assessment following technical guidelines, this study did not quantify the mitigating effects of adaptation measures (e.g., public education or cooling infrastructure).

Conflicts of interest: No conflicts of interest.

Ethical statement: This study did not involve human subjects, animal experiments, informed consent, private data, or any other content requiring an ethical review. The authors declare that the research was conducted in compliance with academic norms and that the data were authentic and reliable.

Funding: Supported by the National Natural Science Foundation of China (42305196, 42071433, 82241051) and the Special Foundation of Basic

Science and Technology Resources Survey of the Ministry of Science and Technology of China (2017FY101204).

doi: 10.46234/ccdcw2026.065

[#] Corresponding author: Tiantian Li, litiantian@nieh.chinacdc.cn.

[1] National Key Laboratory of Intelligent Tracking and Forecasting for Infectious Diseases, China CDC Key Laboratory of Environment and Population Health, China Meteorological Administration Key Laboratory of Meteorological Medicine and Health, National Institute of Environmental Health, Chinese Center for Disease Control and Prevention & Chinese Academy of Preventive Medicine, Beijing, China; [2] School of Environmental Science and Engineering, Nanjing University of Information Science & Technology, Nanjing City, Jiangsu Province, China.

Submitted: September 11, 2025
Accepted: March 01, 2026
Issued: April 03, 2026

REFERENCES

1. World Meteorological Organization (WMO). State of the global climate 2023. Geneva: WMO; 2024 Mar. Report No.: 1347.
2. National Climate Center, China Meteorological Administration. 2023 China climate bulletin. Beijing: China Meteorological Press. 2024; p. 66.
3. Zhao Q, Li SS, Ye TT, Wu Y, Gasparrini A, Tong SL, et al. Global, regional, and national burden of heatwave-related mortality from 1990 to 2019: A three-stage modelling study. PLoS Med 2024;21(5):e1004364. https://doi.org/10.1371/journal.pmed.1004364.
4. Yin P, Chen RJ, Wang LJ, Liu C, Niu Y, Wang W, et al. The added effects of heatwaves on cause-specific mortality: A nationwide analysis in 272 Chinese cities. Environ Int 2018;121(Pt 1):898-905. http://dx.doi.org/10.1016/j.envint.2018.10.016.
5. Anderson GB, Bell ML. Heat waves in the United States: Mortality risk during heat waves and effect modification by heat wave characteristics in 43 U. S. communities. Environ Health Perspect 2011;119(2):210 – 8. https://doi.org/10.1289/ehp.1002313.
6. Sun ZY, Chen C, Yan ML, Shi WY, Wang JN, Ban J, et al. Heat wave characteristics, mortality and effect modification by temperature zones: A time-series study in 130 counties of China. Int J Epidemiol 2020;49(6):1813 – 22. https://doi.org/10.1093/ije/dyaa104.
7. Du H, Yan ML, Liu X, Zhong Y, Ban J, Lu KL, et al. Exposure to concurrent heatwaves and ozone pollution and associations with mortality risk: A nationwide study in China. Environ Health Perspect 2024;132(4):47012. https://doi.org/10.1289/EHP13790.
8. Choi EY, Ailshire JA. Ambient outdoor heat and accelerated epigenetic aging among older adults in the US. Sci Adv 2025;11(9):eadr0616. https://doi.org/10.1126/sciadv.adr0616.
9. Chaseling GK, Uchmanowicz I, Bäck M, Miró Ò, Tokmakova M, Ljungman P, et al. Heat extremes and cardiovascular diseases: a scientific statement of the Association of Cardiovascular Nursing & Allied Professions, Association for Acute Cardiovascular Care, European Association of Preventive Cardiology, Heart Failure Association, European Heart Rhythm Association of the ESC, the ESC Council on Hypertension, the ESC Council on Stroke, and the ESC Working Group on Cardiovascular Pharmacotherapy. Eur Heart J 2025;46(30):2950 – 8. https://doi.org/10.1093/eurheartj/ehaf326.

SUPPLEMENTARY MATERIAL

SUPPLEMENTARY TABLE S1. List of 36 cities in northern China included in the study.

PLADs	City	Average of daily mean temperatures (℃)
Beijing	/	26.6±3.6
Tianjin	/	28.0±3.0
Hebei	Baoding	27.6±3.6
Hebei	Cangzhou	28.3±3.0
Hebei	Chengde	21.8±4.0
Hebei	Handan	27.2±3.4
Hebei	Hengshui	28.3±2.9
Hebei	Langfang	28.5±3.1
Hebei	Qinhuangdao	24.3±2.6
Hebei	Shijiazhuang	27.5±3.2
Hebei	Tangshan	26.4±2.9
Hebei	Xingtai	27.4±3.1
Hebei	Zhangjiakou	20.6±4.0
Shanxi	Datong	20.1±2.9
Shanxi	Jincheng	21.8±2.9
Shanxi	Jinzhong	21.4±2.6
Shanxi	Linfen	21.9±3.0
Shanxi	Lüliang	20.8±2.7
Shanxi	Shuozhou	19.7±2.6
Shanxi	Taiyuan	21.7±2.8
Shanxi	Xinzhou	19.5±2.8
Shanxi	Yangquan	22.4±2.6
Shanxi	Yuncheng	22.9±3.2
Shanxi	Changzhi	21.1±2.6
Inner Mongolia	Alxa League	25.5±3.3
Inner Mongolia	Bayannur	23.3±3.2
Inner Mongolia	Baotou	21.4±3.3
Inner Mongolia	Chifeng	21.8±5.0
Inner Mongolia	Ordos	22.0±2.7
Inner Mongolia	Hohhot	20.7±3.0
Inner Mongolia	Hulunbuir	17.5±4.0
Inner Mongolia	Tongliao	22.8±4.6
Inner Mongolia	Wuhai	24.0±2.9
Inner Mongolia	Ulanqab	19.2±3.7
Inner Mongolia	Xilingol League	20.0±5.2
Inner Mongolia	Hinggan League	19.7±4.4

Note: "/" represents a municipality directly under the central government without a corresponding municipal division.
Abbreviation: PLAD=provincial-level administrative division.

SUPPLEMENTARY TABLE S2. Sensitivity analysis of heat wave days and excess deaths based on exposure-response parameters in the temperate monsoon zone.

Population	Temperate Monsoon Zone	
	Number of heat wave days	Excess Deaths
Total population	1,803	1,308 (754, 1,945)
Male		756 (436,1,124)
Female		551 (318, 820)
0–64 years old		313 (181,466)
≥65 years old		1,011 (583, 1,504)

Note: The results using the region-specific exposure-response parameters for the Temperate Monsoon Zone (where Northern China is located) were derived from Yin et al. (*1*), while maintaining the primary heat wave definition (97.5th percentile, duration ≥2 days).

Preplanned Studies

Differences in Major Causes of Death and Disease Burden Among Residents of Kashin-Beck Disease Endemic and Non-Endemic Areas — Heilongjiang Province, China, 2024

Zhifeng Xing[1,2,&]; Yuqian Song[3,&]; Songyao Zhang[1]; Zewen Wang[4]; Shichun Yan[2]; Ying Wei[5]; Xue Han[2]; Shihui Yin[2]; Jun Yu[1,#]

Summary

What is already known about this topic?

Kashin-Beck disease (KBD) imposes a heavy burden on both patients and their families. However, there are no reports on the health disparities between residents with long-term exposure to KBD risk factors in endemic and non-endemic areas.

What is added by this report?

For ischemic heart diseases, the age-standardized mortality rates (ASMR) were significantly higher in endemic areas, particularly among males, residents aged ≥65 years, and residents in economically developed regions. For malignant neoplasms of the digestive organs, ASMR was higher in endemic areas, and a significant difference in ASMR between the two areas was observed in females. For cerebral infarction, the ASMR was significantly lower in endemic areas, particularly among residents in economically developed regions. The rate of life lost due to ischemic heart diseases and malignant neoplasms of digestive organs was relatively high in endemic areas, while the rate due to cerebral infarction was relatively high in non-endemic areas.

What are the implications for public health practice?

These findings provide scientific evidence for optimizing comprehensive prevention and control strategies for endemic diseases, and strengthening interventions for key diseases.

ABSTRACT

Introduction: This study compared the major causes of death and disease burden in Kashin-Beck disease (KBD) endemic and non-endemic areas of Heilongjiang Province in 2024.

Methods: Data were obtained from the National Disease Surveillance Point system. Age-standardized mortality rates (ASMR), rate ratio, cause-eliminated life expectancy, potential gains in life expectancy, and the rate of life lost were calculated.

Results: The ASMR for ischemic heart disease was higher in endemic areas, whereas cerebral infarction showed a lower ASMR. For ischemic heart diseases, the ASMR was significantly higher in endemic areas, particularly among males [risk ratio (*RR*)=2.79, 95% confidence interval (*CI*): 1.77, 5.38], residents aged ≥ 65 years (*RR*=2.17, 95% *CI*: 1.52, 3.39) and residents in economically developed regions (*RR*=3.00, 95% *CI*: 1.90, 5.93). For malignant neoplasms of digestive organs, the ASMR was higher in endemic areas than that in non-endemic areas, and a significant difference in ASMR between the two areas was observed in females (*RR*=4.14, 95% *CI*: 1.63, 16.30). For cerebral infarction, the ASMR was significantly lower in endemic areas than that in non-endemic areas, particularly among residents in economically developed regions (*RR*=0.32, 95% *CI*: 0.20, 0.55). The rates of life lost due to ischemic heart disease, cerebral infarction, and malignant neoplasms of the digestive organs in endemic areas were 11.32%, 1.42%, and 1.84%, respectively, compared with 4.22%, 6.36%, and 1.41% in non-endemic areas, respectively.

Conclusion: These findings provide evidence for optimizing comprehensive prevention and control strategies for endemic diseases and strengthening interventions.

Kashin-Beck disease (KBD) is an endemic, disabling osteoarticular disorder of unknown etiology. Mild cases present with joint pain, swelling, deformity, and limited limb mobility, whereas severe cases manifest as brachydactyly and dwarfism, leading to a loss of labor capacity (*1*). This disease imposes a heavy burden on patients and their families (*2*).

Heilongjiang Province, China, is heavily affected by KBD. Environmental risk factors (ERFs) such as selenium deficiency and T-2 toxin are primary contributors to KBD (*3*–*4*). However, there are no reports on health disparities between residents with long-term exposure in endemic areas and those in non-endemic areas.

All administrative villages in Heilongjiang Province were classified according to KBD endemic areas criteria, defined as follows: 1) KBD endemic areas (hereafter termed endemic areas): Residents of clinical I degrees or higher prevalence exceeding 5%, and children aged 7–12 exhibiting multiple, symmetrical epiphyseal changes on hand radiographs. Endemic areas were further classified as: mild endemic areas (prevalence of the local residents of clinical I degrees and above or X-ray detection rate ≤10% in 7–12-year-old children), moderate endemic areas (prevalence of the local residents of clinical I degrees and above or X-ray detection rate >10% and ≤20% in 7–12-year-old children), and severe endemic areas (prevalence of the local residents of clinical I degrees and above or X-ray detection rate >20% in 7–12-year-old children); 2) Non-endemic areas: Administrative villages not meeting the criteria for endemic areas. Heilongjiang Province had 9,073 administrative villages, including 7,199 non-endemic areas, 1,405 mild endemic areas, 148 moderate endemic areas, and 321 severe endemic areas in 2024.

Stratified random sampling was employed to select 165 administrative villages, including 47 mild endemic areas, 42 moderate endemic areas, 45 severe endemic areas, and 31 non-endemic areas. The administrative villages were classified into economically developed and underdeveloped regions based on the regional gross domestic product (GDP). Causes of death were obtained from the National Disease Surveillance Point (DSP) System. In April 2004, Heilongjiang Province officially launched online direct reporting of individual death case information across the province, relying on the Disease Surveillance Information Report Management System (Major Epidemic Online Direct Reporting System). By 2007, this system was connected to the National Cause of Death Registration Reporting Information System, thereby achieving full online direct reporting of individual death cases in all counties and districts across the province. All causes of death were identified and classified according to the International Classification of Diseases ICD-10 standard. Information on the 2024 permanent population (defined as individuals who had lived in the sampled administrative villages for more than six months) was collected through a complete census. The census covered all types of residential premises within the jurisdiction. Duplicate registrations and erroneous information were eliminated using multiple verification methods, including logical verification and cross-departmental data comparison.

Age-standardized mortality rates (ASMRs) were calculated based on 2020 Chinese National Census data. The Poisson parametric bootstrap method was used to compare rate ratios (*RR*s), 95% confidence intervals (*CI*s), and *P*. The unit of analysis was the administrative village included in the study. Point estimates of *RR* were derived directly by calculating the ratio of ASMRs between the compared areas, whereas group-specific resampling with replacement (sample size matching the original) was performed to estimate the 95% *CI*s and *P*. Poisson regression analyses were performed for the composite major causes of death, the three major causes of death, and their main subtypes to verify the robustness of the results. The false discovery rate (FDR) method was used to adjust the *P* across all tables. Cause-eliminated life expectancy (CELE) was calculated using the life table method. This reflects the potential increase in a population's average life expectancy if a specific cause of death is eliminated. Potential gains in life expectancy (PGLEs) represented the increase in life expectancy following the elimination of a specific cause of death (PGLEs = CELE – life expectancy) and served as an indicator of population life expectancy gains. The rate of life lost refers to the proportion of the total life expectancy lost due to a specific cause of death [rate of life loss = (potential additional years of life expectancy) × 100%]. CELE was truncated at age 95.

The baseline characteristics of the participants were reported descriptively, with frequencies (percentages) for binary variables and medians (interquartile range) for continuous variables. Intergroup comparisons were performed using the Mann-Whitney U, Kruskal-Wallis, χ^2 tests, or Fisher's exact tests. All analyses were conducted using the R software (version 4.4.3; R Foundation for Statistical Computing, Vienna, Austria). A two-sided $P<0.05$ was considered statistically significant.

The primary causes of death in the general population were heart diseases (31.94%), malignant neoplasms (25.71%), and cerebrovascular diseases (24.98%), which were the major causes of mortality (Table 1).

The ASMR for the composite major causes of death

TABLE 1. General characteristics of decedents by area in Heilongjiang Province, 2024.

Variables	Total (*n*=1,365)	Endemic areas (*n*=1,128)	Non-endemic areas (*n*=237)	$P_{\text{Endemic areas vs. Non-endemic areas}}$	Mild endemic areas (*n*=388)	Moderate endemic areas (*n*=487)	Severe endemic areas (*n*=253)	$P_{\text{Mild endemic areas vs. Moderate endemic areas vs. Severe endemic areas}}$*
Age (years)	73 (65–80)	73 (65–80)	72 (62–79)	0.261	72 (66–79)	74 (65–81)	73 (62–79)	0.334
Sex (*n*, %)				0.334				0.880
Male	815 (59.71)	681 (60.37)	134 (56.54)		236 (60.82)	290 (59.55)	155 (61.26)	
Female	550 (40.29)	447 (39.63)	103 (43.46)		152 (39.18)	197 (40.45)	98 (38.74)	
Economic conditions (*n*, %)				<0.001				<0.001
Developed regions	795 (58.24)	690 (61.17)	105 (43.30)		196 (50.52)	335 (68.79)	159 (62.85)	
Underdeveloped regions	570 (41.76)	438 (38.83)	132 (55.70)		192 (49.48)	152 (31.21)	94 (37.15)	
Causes of death (*n*, %)				<0.001				<0.001
Heart diseases	436 (31.94)	380 (33.69)	56 (23.63)		114 (29.38)	162 (33.26)	104 (41.11)	
Malignant neoplasms	351 (25.71)	298 (26.42)	53 (22.63)		94 (24.23)	137 (28.13)	67 (26.48)	
Cerebrovascular diseases	341 (24.98)	259 (22.96)	82 (34.60)		93 (23.97)	114 (23.41)	52 (20.55)	
Diseases of the respiratory system	81 (5.93)	67 (5.94)	14 (5.91)		34 (8.76)	28 (5.75)	5 (1.98)	
External causes of mortality	36 (2.64)	29 (2.57)	7 (2.95)		12 (3.09)	9 (1.85)	8 (3.16)	
Diseases of the digestive system	29 (2.12)	24 (2.13)	5 (2.11)		6 (1.55)	13 (2.67)	5 (1.98)	
Endocrine, nutritional, and metabolic diseases	27 (1.98)	23 (2.04)	4 (1.69)		7 (1.80)	9 (1.85)	7 (2.77)	
Diseases of the nervous system	20 (1.47)	19 (1.68)	1 (0.42)		17 (4.38)	2 (0.41)	0 (0)	
Certain infectious and parasitic diseases	8 (0.59)	5 (0.44)	3 (1.27)		0 (0)	3 (0.62)	2 (0.79)	
Diseases of the genitourinary system	6 (0.44)	4 (0.35)	2 (0.84)		1 (0.26)	2 (0.41)	1 (0.40)	
Mental and behavioral disorders	3 (0.22)	2 (0.18)	1 (0.42)		1 (0.26)	1 (0.21)	0 (0)	
Diseases of the blood and blood-forming organs, and certain disorders involving the immune mechanism	2 (0.15)	2 (0.18)	0 (0)		2 (0.52)	0 (0)	0 (0)	
Congenital malformations, deformations, and chromosomal abnormalities	1 (0.07)	1 (0.09)	0 (0)		0 (0)	1 (0.21)	0 (0)	
Certain conditions originating in the perinatal period	1 (0.07)	1 (0.09)	0 (0)		0 (0)	0 (0)	1 (0.40)	
Undetermined diseases	10 (0.73)	3 (0.27)	7 (2.95)		3 (0.77)	0 (0)	0 (0)	
Other diseases	13 (0.95)	11 (0.98)	2 (0.84)		4 (1.03)	6 (1.23)	1 (0.40)	

Note: Parentheses content explanation: In the "Age (years)" row: Values in parentheses represent the interquartile range (*IQR*) of age distribution. In the "Sex (*n*, %)" and "Economic conditions (*n*, %)" rows: Values in parentheses represent the percentage (%) of each category within the total number of decedents in the corresponding group. In the "Causes of death (*n*, %)" rows: Values in parentheses represent the percentage (%) of each cause of death within the total number of decedents in the corresponding group.

* *P* represents the overall significance of differences in the general characteristics of the decedents across mild, moderate, and severe endemic areas. Continuous variables were compared using the Kruskal–Wallis test, and categorical variables were compared using χ^2 test. All *P* were adjusted.

Abbreviation: ASMR=age-standardized mortality rate; *RR*=rate ratio.

was higher in endemic areas than that in non-endemic areas; however, the difference was not statistically significant. The ASMRs for heart diseases (*RR*=1.80, 95% *CI*: 1.35, 2.54) and ischemic heart diseases (*RR*=1.98, 95% *CI*: 1.46, 2.87) were significantly higher in endemic areas, while cerebrovascular diseases (*RR*=0.62, 95% *CI*: 0.47, 0.85) and cerebral infarction (*RR*=0.52, 95% *CI*: 0.37, 0.79) showed lower ASMRs in endemic areas. The ASMRs for malignancy and malignant neoplasms of the digestive organs were higher in endemic areas, but the difference was not significant. The ASMR for the composite major causes of death in moderate endemic areas was significantly higher than that in non-endemic areas. The ASMRs for heart diseases and ischemic heart diseases were significantly higher in all endemic areas than those in non-endemic areas. The ASMRs for malignant neoplasms and malignant neoplasms of the digestive system were significantly higher in moderate endemic areas, and the ASMRs for cerebrovascular disease and cerebral infarction were significantly lower in mild and severe endemic areas (Table 2). The results of the sensitivity analysis were consistent with these findings (Supplementary Table S1, available at https://weekly.chinacdc.cn/).

The stratified analysis showed that the ASMR for ischemic heart diseases (*RR*=2.79, 95% *CI*: 1.77, 5.38) was significantly higher in endemic areas than that in non-endemic areas among males, while the ASMR for malignant neoplasms of digestive organs (*RR*=4.14, 95% *CI*: 1.63, 16.30) was significantly higher than that in non-endemic areas among females. The ASMRs for ischemic heart disease were consistently higher than those in non-endemic areas among males, while the ASMR for cerebral infarction in severe areas was significantly lower than that in non-endemic areas. Among women, the ASMR for malignant neoplasms of the digestive organs in moderate endemic areas was significantly higher than that in non-endemic areas, and the ASMR for cerebral infarction in severe endemic areas was significantly lower than that in non-endemic areas. Among residents aged <65 years, no significant differences in ASMRs for all-cause deaths were observed between endemic and non-endemic areas. Among residents aged ≥65 years, the ASMR for ischemic heart diseases (*RR*=2.17, 95% *CI*: 1.52, 3.39) was significantly higher in endemic areas than that in non-endemic areas. In different endemic areas, the ASMRs for ischemic heart disease were consistently higher than those in non-endemic areas among residents aged ≥65 years, and the ASMRs for cerebral infarction in severe endemic areas were significantly lower than those in non-endemic areas. In endemic areas, the ASMR for ischemic heart diseases (*RR*=3.00, 95% *CI*: 1.90, 5.93) was significantly higher than that in non-endemic areas among residents in economically developed regions, and the ASMR for cerebral infarction (*RR*=0.32, 95% *CI*: 0.20, 0.55) was significantly lower than that in non-endemic areas. Among residents of economically underdeveloped regions, no significant differences in ASMRs for all causes of death were observed between endemic and non-endemic areas. The ASMRs for ischemic heart disease were consistently higher among residents in economically developed regions, while the ASMRs for cerebral infarction in mild and severe areas were significantly lower than those in non-endemic areas. The ASMR for malignant neoplasms of the digestive organs in moderate endemic areas was significantly higher than that in non-endemic areas among residents of economically developed regions (Supplementary Table S2, available at https://weekly.chinacdc.cn/). The rates of life lost due to ischemic heart disease, cerebral infarction, and malignant neoplasms of the digestive organs in endemic areas were 11.32%, 1.42%, and 1.84%, respectively, compared to 4.22%, 6.36%, and 1.41% in non-endemic areas (Table 3).

DISCUSSION

ERFs play pivotal roles in the development and progression of KBD and also influence the onset and progression of various diseases through multiple pathways, including oxidative stress and inflammatory responses (*5*–*6*). The high ASMR of ischemic heart disease in endemic areas may be related to selenium deficiency, which induces cellular oxidative stress and inflammatory factor expression (*7*). On the other hand, T-2 toxin can also directly impair the function and structure of cardiomyocytes through its cardiotoxicity (*8*–*9*). The elevated ASMR in malignant neoplasms of the digestive organs may be associated with direct damage to the gastrointestinal tract by the T-2 toxin (*10*). The ASMR for cerebral infarction in endemic areas was significantly lower than that in non-endemic areas, which may be attributable to competing risks posed by the higher ASMRs of heart disease and malignant neoplasms in endemic areas. In addition, local dietary structure, lifestyle, and public health interventions may also reduce the ASMR of this disease. The higher smoking prevalence in males (*11*), combined with exposure to high-level ERFs, further

TABLE 2. ASMRs and *RR*s for major causes of death and subtypes by areas in Heilongjiang Province, 2024.

Causes of death	$ASMR_{Total}$ (per 100,000)	$ASMR_{Endemic\ areas}$ (per 100,000)	$ASMR_{Non\text{-}endemic\ areas}$ (per 100,000)	$ASMR_{Mild\ endemic\ areas}$ (per 100,000)	$ASMR_{Moderate\ endemic\ areas}$ (per 100,000)	$ASMR_{Severe\ endemic\ areas}$ (per 100,000)	$RR_{Endemic\ areas\ vs.\ Non\text{-}endemic\ areas}$	$RR_{Mild\ endemic\ areas\ vs.\ Non\text{-}endemic\ areas}$	$RR_{Moderate\ endemic\ areas\ vs.\ Non\text{-}endemic\ areas}$	$RR_{Severe\ endemic\ areas\ vs.\ Non\text{-}endemic\ areas}$
Major causes of death	416.30	430.98	356.37	404.71	508.75	356.37	1.21 (1.02−1.45)	1.14 (0.93−1.41)	1.43 (1.18−1.73)***	1.00 (0.81−1.24)
Heart diseases	185.16	202.49	112.77	186.02	224.39	190.24	1.80 (1.35−2.54)***	1.65 (1.17−2.41)*	1.99 (1.45−2.84)***	1.69 (1.19−2.47)**
Ischemic heart diseases	169.13	187.10	94.39	176.65	197.41	185.17	1.98 (1.46−2.87)***	1.87 (1.31−2.83)***	2.09 (1.49−3.14)***	1.96 (1.37−2.98)**
Hypertensive diseases	6.94	6.16	10.73	4.60	10.21	2.01	0.57 (0.21−2.94)	0.43 (0.00−2.40)	0.95 (0.25−4.91)	0.19 (0−1.14)
Pulmonary heart disease and diseases of pulmonary circulation	4.71	5.35	1.76	2.42	10.28	1.46	3.04 (0.60−4.85)	1.37 (0.00−3.39)	5.84 (0.96−10.10)	0.83 (0.00−2.49)
Cardiac arrhythmias	3.17	2.37	5.90	1.18	3.78	1.59	0.40 (0.06−1.31)	0.20 (0−1.00)	0.64 (0−2.20)	0.27 (0−1.35)
Cardiomyopathy	0.48	0.60	0	0	1.40	0	−	−	−	−
Chronic rheumatic heart diseases	0.42	0.53	0	0	1.30	0	−	−	−	−
Heart failure	0.31	0.38	0	1.18	0	0	−	−	−	−
Cerebrovascular diseases	98.12	88.18	141.86	87.38	110.86	61.45	0.62 (0.47−0.85)*	0.62 (0.42−0.90)*	0.78 (0.56−1.10)	0.43 (0.28−0.65)**
Cerebral infarction	59.48	50.74	98.45	49.12	69.01	29.06	0.52 (0.37−0.79)**	0.50 (0.30−0.80)*	0.70 (0.46−1.09)	0.30 (0.16−0.51)***
Intracerebral hemorrhage	38.20	36.92	43.41	36.52	41.85	32.40	0.85 (0.54−1.50)	0.84 (0.44−1.59)	0.96 (0.57−1.75)	0.75 (0.39−1.43)
Cerebral aneurysm	0.43	0.53	0	1.75	0	0	−	−	−	−
Malignant neoplasms	133.02	140.31	101.73	131.31	173.50	104.68	1.38 (1.03−1.92)	1.29 (0.91−1.88)	1.71 (1.25−2.44)**	1.03 (0.71−1.51)
Malignant neoplasms of digestive organs	65.01	69.59	44.56	69.08	86.61	46.71	1.56 (1.02−2.71)	1.55 (0.93−2.78)	1.94 (1.21−3.40)*	1.05 (0.59−1.93)
Malignant neoplasms of respiratory and intrathoracic organs	48.42	48.35	49.63	46.23	55.25	41.75	0.97 (0.64−1.63)	0.93 (0.54−1.64)	1.11 (0.68−1.95)	0.84 (0.47−1.53)
Malignant neoplasms of urinary tract	5.10	5.90	1.78	4.41	10.58	1.27	3.32 (0.65−5.35)	2.48 (0−5.86)	5.95 (1.01−10.30)	0.72 (0−2.15)
Malignant neoplasms of female genital organs	4.05	4.05	3.99	0	6.50	5.07	1.01 (0.25−3.18)	−	1.63 (0.29−5.45)	1.27 (0−4.89)
Malignant neoplasms of lymphoid, hematopoietic, and related tissue	3.10	3.39	1.78	1.58	2.29	6.88	1.91 (0.30−3.24)	0.89 (0−2.67)	1.29 (0−2.97)	3.88 (0.38−7.63)
Malignant neoplasms of eye, brain, and other parts of central nervous system	2.13	2.60	0	1.18	4.24	1.50	−	−	−	−
Malignant neoplasms of breast	1.65	2.04	0	3.09	1.40	1.50	−	−	−	−
Malignant neoplasms of thyroid and other endocrine glands	1.16	1.42	0	1.75	2.41	0	−	−	−	−
Malignant neoplasms of bone and articular cartilage	1.06	1.30	0	1.24	2.41	0	−	−	−	−
Malignant neoplasms of lip, oral cavity, and pharynx	0.72	0.88	0	2.76	0	0	−	−	−	−
Malignant neoplasms of mesothelial and soft tissue	0.62	0.78	0	0	1.83	0	−	−	−	−

Note: "−" denotes missing *RR* due to zero ASMR in numerator or denominator.

* $P<0.05$; ** $P<0.01$; *** $P<0.001$ (adjusted).

Abbreviation: ASMR=age-standardized mortality rate; *RR*=rate ratio.

TABLE 3. CELE, PGLEs and the rate of life lost for major causes of death and subtypes by areas in Heilongjiang Province, 2024.

Causes of death	CELE (years)						PGLEs (years)						The rate of life lost (%)					
	Total	Endemic areas	Non-endemic areas	Mild endemic areas	Moderate endemic areas	Severe endemic areas	Total	Endemic areas	Non-endemic areas	Mild endemic areas	Moderate endemic areas	Severe endemic areas	Total	Endemic areas	Non-endemic areas	Mild endemic areas	Moderate endemic areas	Severe endemic areas
Heart diseases	92.52	93.23	90.21	87.05	92.47	95.00	9.90	11.02	5.50	5.40	10.91	9.27	11.98	13.41	6.49	6.61	13.38	10.82
Ischemic heart diseases	90.75	91.51	88.28	86.33	90.00	95.00	8.13	9.31	3.57	4.68	8.44	9.27	9.84	11.32	4.22	5.73	10.35	10.82
Hypertensive diseases	82.80	82.35	84.99	81.74	81.79	85.79	0.17	0.15	0.28	0.09	0.23	0.06	0.21	0.18	0.33	0.11	0.28	0.07
Pulmonary heart disease and diseases of pulmonary circulation	82.75	82.34	84.75	81.69	81.79	85.77	0.13	0.13	0.04	0.04	0.23	0.04	0.15	0.16	0.05	0.05	0.28	0.05
Cardiac arrhythmias	82.72	82.25	85.21	81.67	81.64	85.76	0.10	0.05	0.50	0.02	0.08	0.03	0.12	0.06	0.59	0.02	0.10	0.04
Cardiomyopathy	82.64	82.22	84.71	81.65	81.59	85.73	0.01	0.01	0	0	0.03	0	0.01	0.02	0	0	0.04	0
Chronic rheumatic heart diseases	82.64	82.22	84.71	81.65	81.60	85.73	0.01	0.02	0	0	0.04	0	0.02	0.02	0	0	0.05	0
Heart failure	82.63	82.21	84.71	81.67	81.56	85.73	0.01	0.01	0	0.02	0	0	0.01	0.01	0	0.02	0	0
Cerebrovascular diseases	86.60	85.42	95.00	84.91	84.63	89.23	3.98	3.22	10.29	3.26	3.07	3.50	4.81	3.92	12.15	3.99	3.77	4.09
Cerebral infarction	84.21	83.37	90.10	82.58	82.95	86.85	1.59	1.17	5.39	0.93	1.39	1.13	1.92	1.42	6.36	1.14	1.71	1.32
Intracerebral Hemorrhage	83.50	83.01	86.01	82.40	82.28	86.95	0.88	0.80	1.30	0.75	0.72	1.22	1.06	0.98	1.53	0.91	0.88	1.43
Cerebral aneurysm	82.63	82.21	84.71	81.68	81.56	85.73	0.01	0.01	0	0.03	0	0	0.01	0.01	0	0.04	0	0
Malignant neoplasms	85.90	85.51	87.74	84.25	85.63	88.45	3.27	3.31	3.03	2.60	4.07	2.72	3.96	4.03	3.57	3.19	5.00	3.17
Malignant neoplasms of digestive organs	84.09	83.71	85.91	82.89	83.38	86.93	1.46	1.51	1.20	1.24	1.82	1.21	1.77	1.84	1.41	1.52	2.24	1.41
Malignant neoplasms of respiratory and intrathoracic organs	83.63	83.19	85.80	82.44	82.68	86.74	1.00	0.99	1.09	0.78	1.12	1.01	1.21	1.20	1.29	0.96	1.37	1.18
Malignant neoplasms of urinary tract	82.78	82.38	84.75	81.75	81.82	85.75	0.16	0.17	0.04	0.09	0.26	0.03	0.19	0.21	0.05	0.12	0.32	0.03
Malignant neoplasms of female genital organs	82.71	82.30	84.79	81.65	81.69	85.87	0.09	0.09	0.08	0	0.13	0.14	0.11	0.11	0.09	0	0.16	0.17
Malignant neoplasms of lyphoid, hematopoietic and related tissue	82.69	82.27	84.75	81.68	81.60	85.91	0.06	0.07	0.04	0.02	0.04	0.18	0.08	0.08	0.05	0.03	0.05	0.21
Malignant neoplasms of eye, brain and other parts of central nervous system	82.67	82.26	84.71	81.67	81.65	85.73	0.05	0.06	0	0.02	0.09	0	0.06	0.07	0	0.02	0.11	0

Continued

Causes of death	CELE (years)					PGLEs (years)					The rate of life lost (%)				
	Total	Endemic areas	Non-endemic areas	Mild endemic areas	Moderate endemic areas	Severe endemic areas	Total	Endemic areas	Non-endemic areas	Mild endemic areas	Moderate endemic areas	Severe endemic areas	Total	Endemic areas	Non-endemic areas	Mild endemic areas	Moderate endemic areas	Severe endemic areas
Malignant neoplasms of breast	82.66	82.25	84.71	81.73	81.59	85.75	0.04	0.05	0	0.08	0.03	0.03	0.04	0.06	0	0.10	0.04	0.03
Malignant neoplasms of thyroid and other endocrine glands	82.65	82.23	84.71	81.68	81.60	85.73	0.02	0.02	0	0.03	0.04	0	0.03	0.03	0	0.04	0.05	0
Malignant neoplasms of bone and articular cartilage	82.64	82.23	84.71	81.67	81.60	85.73	0.02	0.02	0	0.02	0.04	0	0.02	0.03	0	0.03	0.05	0
Malignant neoplasms of lip, oral cavity, and pharynx	82.64	82.22	84.71	81.69	81.56	85.73	0.01	0.01	0	0.04	0	0	0.01	0.02	0	0.05	0	0
Malignant neoplasms of mesothelial and soft tissue	82.65	82.23	84.71	81.65	81.62	85.73	0.03	0.03	0	0	0.06	0	0.03	0.04	0	0	0.07	0

Abbreviation: CELE=cause-eliminated life expectancy; PGLEs=potential gains in life expectancy.

elevates the mortality risk of ischemic heart disease among male residents in endemic areas. Various carcinogens in tobacco products, such as tobacco-specific nitrosamines, can jointly promote the occurrence and development of malignant neoplasms through mechanisms such as the induction of DNA adduct formation, gene mutations, and chronic inflammation (*12–13*). The magnitude of this effect may mask the impact of ERFs, resulting in no difference in ASMR for malignant neoplasms of the digestive organs between the two areas. Aging disrupts the body's oxidative and antioxidant balance, and ERFs exacerbate oxidative stress. This synergy results in a higher ASMR for multiple causes of death among elderly residents in KBD-endemic areas than in non-endemic areas (*14*). Compared with economically developed regions, less developed areas may consume more grain. Phenolic compounds in these grains possess antioxidant and anti-inflammatory properties that can reduce the risk of cardiovascular diseases, malignant neoplasms, and other conditions (*15*), thereby mitigating the impact of ERFs. Consequently, no significant differences in ASMR across causes of death were observed between endemic and non-endemic areas. Furthermore, ischemic heart diseases and malignant neoplasms of the digestive organs caused greater rates of loss of life in endemic areas, whereas cerebral infarction had a more pronounced impact in non-endemic areas. This pattern aligns with the previous findings.

This study had a few limitations. First, the use of stratified sampling carries the risk of sampling errors, which could limit the generalizability of our findings to the overall population of Heilongjiang Province. Second, the data were based on surveillance reports, which may contain underreporting or misreporting, which could compromise the accuracy.

In summary, the ASMR of ischemic heart diseases was significantly higher in endemic areas than that in non-endemic areas, particularly among males, residents aged ≥65 years and residents in economically developed regions. For malignant neoplasms of the digestive organs, ASMR was higher in endemic areas, with a statistically significant difference observed in females between the two regions. For cerebral infarction, ASMR was significantly lower in endemic areas than that in non-endemic areas among residents in economically developed regions. The rate of life lost due to ischemic heart disease and malignant neoplasms of the digestive organs was relatively high in endemic areas, whereas the rate due to cerebral infarction was

relatively high in non-endemic areas. These findings provide scientific evidence for optimizing comprehensive prevention and control strategies for endemic diseases and strengthening interventions for key diseases as well as practical insights for promoting regional health equity. Identifying high-risk populations and implementing targeted interventions can effectively protect the health of vulnerable groups and improve their overall social wellbeing.

Conflicts of interest: No conflicts of interest.

Ethical statement: Approved by the Ethics Committee of Harbin Medical University, with approval number (hrbmuecdc20221102). This study was conducted in accordance with the ethical guidelines and principles outlined in the Declaration of Helsinki.

Funding: Supported by the National Key Research and Development Program of China (grant number 2022YFC2503101).

doi: 10.46234/ccdcw2026.066

[#] Corresponding author: Jun Yu, 400049@hrbmu.edu.cn.

[1] Institute for Kashin-Beck Disease Control and Prevention, National Center for Endemic Disease Control, Chinese Center for Disease Control and Prevention, Harbin Medical University, Harbin City, Heilongjiang Province, China; [2] Heilongjiang Provincial Center for Disease Control and Prevention, Harbin City, Heilongjiang Province, China; [3] School of Public Health, Harbin Medical University, Harbin City, Heilongjiang Province, China; [4] School of Future Technology, Harbin Institute of Technology, Harbin City, Heilongjiang Province, China; [5] Heilongjiang Provincial Hospital, Harbin City, Heilongjiang Province, China.

[&] Joint first authors.

Submitted: December 23, 2025
Accepted: March 16, 2026
Issued: April 03, 2026

REFERENCES

1. Yu FF, Zuo J, Sun L, Yu SY, Lei XL, Zhu JH, et al. Animal models of Kashin-Beck disease exposed to environmental risk factors: methods and comparisons. Ecotoxicol Environ Saf 2022;234:113419. https://doi.org/10.1016/j.ecoenv.2022.113419.
2. Wang KW, Yu J, Liu H, Liu YQ, Liu N, Cao YH, et al. Endemic Kashin-Beck disease: a food-sourced osteoarthropathy. Semin Arthritis Rheum 2020;50(2):366 – 72. https://doi.org/10.1016/j.semarthrit.2019.07.014.
3. Li D, Han J, Guo X, Qu C, Yu F, Wu X. The effects of T-2 toxin on the prevalence and development of Kashin-Beck disease in China: a meta-analysis and systematic review. Toxicol Res (Camb). 2016 Feb 18;5(3):731-751. https://doi.org/10.1039/c5tx00377f.
4. Liu L, Luo P, Wen PF, Xu P. Effects of selenium and iodine on Kashin-Beck disease: an updated review. Front Nutr 2024;11:1402559. https://doi.org/10.3389/fnut.2024.1402559.
5. Shimada BK, Alfulaij N, Seale LA. The impact of selenium deficiency on cardiovascular function. Int J Mol Sci 2021;22(19):10713. https://doi.org/10.3390/ijms221910713.
6. Dai CS, Das Gupta S, Wang ZH, Jiang HY, Velkov T, Shen JZ. T-2 toxin and its cardiotoxicity: new insights on the molecular mechanisms and therapeutic implications. Food Chem Toxicol 2022;167:113262. https://doi.org/10.1016/j.fct.2022.113262.
7. Giacconi R, Chiodi L, Boccoli G, Costarelli L, Piacenza F, Provinciali M, et al. Reduced levels of plasma selenium are associated with increased inflammation and cardiovascular disease in an Italian elderly population. Exp Gerontol 2021;145:111219. https://doi.org/10.1016/j.exger.2020.111219.
8. Wang C, He J, Jin H, Xiao HX, Peng SQ, Xie JW, et al. T-2 toxin induces cardiotoxicity by activating ferroptosis and inhibiting heme oxygenase-1. Chemosphere 2023;341:140087. https://doi.org/10.1016/j.chemosphere.2023.140087.
9. Qiao LC, Lin X, Liu HB, Xiang RQ, Zhan JM, Deng FD, et al. T-2 toxin induces cardiac fibrosis by causing metabolic disorders and up-regulating Sirt3/FoxO3α/MnSOD signaling pathway-mediated oxidative stress. J Environ Sci 2025;150:532 – 44. https://doi.org/10.1016/j.jes.2024.03.001.
10. Zhou YF, Feng XH, Ren SJ, Wen GH, Wu J. Research progress in toxicity of T - 2 toxin. Hunan J Anim Sci Vet Med 2025;(2):49-54. http://dx.doi.org/10.3969/j.issn.1006-4907.2025.02.016. (In Chinese).
11. Clinton SK, Giovannucci EL, Hursting SD. The world cancer research fund/American institute for cancer research third expert report on diet, nutrition, physical activity, and cancer: impact and future directions. J Nutr 2020;150(4):663 – 71. https://doi.org/10.1093/jn/nxz268.
12. Hecht SS, Hatsukami DK. Smokeless tobacco and cigarette smoking: chemical mechanisms and cancer prevention. Nat Rev Cancer 2022;22(3):143 – 55. https://doi.org/10.1038/s41568-021-00423-4.
13. S V, Dharmashekara C, Prasad A, Prasad KS, Srinivasa C, GC K, et al. Smoking carcinogens and lung cancer - a review. Asian J Pharm Clin Res 2021;14(1):5 – 12. https://doi.org/10.22159/ajpcr.2021.v14i1.39811.
14. Violi F, Loffredo L, Carnevale R, Pignatelli P, Pastori D. Atherothrombosis and oxidative stress: mechanisms and management in elderly. Antioxid Redox Signal 2017;27(14):1083 – 124. https://doi.org/10.1089/ars.2016.6963.
15. Zhang H, Tsao R. Dietary polyphenols, oxidative stress and antioxidant and anti-inflammatory effects. Curr Opin Food Sci 2016;8:33 – 42. https://doi.org/10.1016/j.cofs.2016.02.002.

SUPPLEMENTARY MATERIALS

SUPPLEMENTARY TABLE S1. ASMRs and *RR*s from Poisson regression analysis for composite major causes of death, three major causes of death, and their main subtypes.

Causes of death	$ASMR_{Total}$ (per 100,000)	$ASMR_{Endemic\ areas}$ (per 100,000)	$ASMR_{Non\text{-}endemic\ areas}$ (per 100,000)	$ASMR_{Mild\ endemic\ areas}$ (per 100,000)	$ASMR_{Moderate\ endemic\ areas}$ (per 100,000)	$ASMR_{Severe\ endemic\ areas}$ (per 100,000)	$RR_{Endemic\ areas\ vs.\ Non\text{-}endemic\ areas}$	$RR_{Mild\ endemic\ areas\ vs.\ Non\text{-}endemic\ areas}$	$RR_{Moderate\ endemic\ areas\ vs.\ Non\text{-}endemic\ areas}$	$RR_{Severe\ endemic\ areas\ vs.\ Non\text{-}endemic\ areas}$
Major causes of death	416.30	427.52	363.83	415.37	496.63	346.25	1.18 (1.00−1.38)	1.14 (0.94−1.38)	1.37 (1.14−1.63)***	0.95 (0.77−1.16)
Heart diseases	185.16	196.32	114.54	191.32	214.15	177.23	1.71 (1.23−2.29)***	1.67 (1.13−2.28)*	1.86 (1.35−2.57)***	1.55 (1.09−2.17)*
Ischemic heart diseases	169.13	181.47	95.39	179.40	189.71	172.41	1.90 (1.42−2.68)***	1.88 (1.37−2.68)***	1.99 (1.43−2.79)***	1.81 (1.25−2.66)***
Cerebrovascular diseases	98.12	89.53	141.00	87.36	111.65	61.79	0.63 (0.49−0.83)***	0.62 (0.46−0.89)*	0.79 (0.66−1.06)	0.44 (0.30−0.63)***
Cerebral infarction	59.48	56.97	96.66	52.64	67.88	42.07	0.59 (0.43−0.87)*	0.54 (0.35−0.89)*	0.70 (0.47−1.08)	0.44 (0.23−0.84)***
Malignant neoplasms	133.02	141.99	105.86	137.08	171.07	107.61	1.34 (1.00−1.87)	1.29 (0.89−1.86)	1.62 (1.17−2.24)*	1.02 (0.71−1.49)
Malignant neoplasms of digestive organs	65.01	68.57	45.55	71.92	82.70	46.13	1.51 (0.96−2.50)	1.58 (1.00−2.75)	1.82 (1.13−3.06)*	1.01 (0.58−1.84)

Note: * $P<0.05$; ** $P<0.01$; *** $P<0.001$ (adjusted).
Abbreviation: ASMR=age-standardized mortality rate; *RR*=rate ratio.

SUPPLEMENTARY TABLE S2. ASMRs and *RR*s for major causes of death and subtypes by sex, age and economic conditions in Heilongjiang Province, 2024.

Variable	Causes of death	$ASMR_{Total}$ (per 100,000)	$ASMR_{Endemic\ areas}$ (per 100,000)	$ASMR_{Non-endemic\ areas}$ (per 100,000)	$ASMR_{Mild\ endemic\ areas}$ (per 100,000)	$ASMR_{Moderate\ endemic\ areas}$ (per 100,000)	$ASMR_{Severe\ endemic\ areas}$ (per 100,000)	$RR_{Endemic\ areas\ vs.\ Non-endemic\ areas}$	$RR_{Mild\ endemic\ areas\ vs.\ Non-endemic\ areas}$	$RR_{Moderate\ endemic\ areas\ vs.\ Non-endemic\ areas}$	$RR_{Severe\ endemic\ areas\ vs.\ Non-endemic\ areas}$
Male	Major causes of death	504.54	518.13	446.81	490.54	610.47	431.32	1.16 (0.93−1.48)	1.10 (0.84−1.45)	1.37 (1.07−1.78)	0.97 (0.73−1.29)
	Heart diseases	210.80	234.84	101.95	202.63	269.91	225.32	2.30 (1.51−3.99)**	1.99 (1.22−3.57)*	2.65 (1.68−4.62)***	2.21 (1.33−3.96)*
	Ischemic heart diseases	189.82	215.15	77.13	188.95	236.21	219.23	2.79 (1.77−5.38)***	2.45 (1.44−4.80)**	3.06 (1.85−5.96)***	2.84 (1.67−5.65)***
	Cerebrovascular diseases	130.74	116.80	194.41	120.64	137.96	87.38	0.60 (0.42−0.92)	0.62 (0.38−1.01)	0.71 (0.47−1.13)	0.45 (0.27−0.75)*
	Cerebral infarction	80.84	69.05	135.93	65.87	90.42	45.26	0.51 (0.32−0.86)	0.49 (0.26−0.90)	0.67 (0.39−1.18)	0.33 (0.15−0.66)*
	Malignant neoplasms	163.00	166.49	150.44	167.27	202.59	118.63	1.11 (0.78−1.69)	1.11 (0.73−1.74)	1.35 (0.92−2.07)	0.79 (0.50−1.28)
	Malignant neoplasms of digestive organs	87.15	89.19	79.91	93.97	111.34	55.23	1.12 (0.70−2.06)	1.18 (0.65−2.29)	1.39 (0.83−2.59)	0.69 (0.34−1.40)
Female	Major causes of death	330.71	345.21	275.36	319.45	410.58	283.12	1.25 (0.97−1.68)	1.16 (0.84−1.61)	1.49 (1.12−2.03)*	1.03 (0.74−1.44)
	Heart diseases	160.11	170.61	120.80	168.67	180.69	157.34	1.41 (0.96−2.32)	1.40 (0.86−2.35)	1.50 (0.97−2.48)	1.30 (0.81−2.19)
	Ischemic heart diseases	148.93	159.56	107.86	163.72	160.34	153.51	1.48 (0.99−2.49)	1.52 (0.93−2.60)	1.49 (0.94−2.54)	1.42 (0.87−2.46)
	Cerebrovascular diseases	67.19	60.27	97.78	54.63	84.26	35.14	0.62 (0.39−1.04)	0.56 (0.29−1.05)	0.86 (0.51−1.52)	0.36 (0.14−0.74)*
	Cerebral infarction	39.48	33.11	67.56	32.56	48.51	13.88	0.49 (0.27−0.97)	0.48 (0.19−1.06)	0.72 (0.36−1.47)	0.21 (0.04−0.55)*
	Malignant neoplasms	103.41	114.32	56.79	96.16	145.63	90.64	2.01 (1.22−4.08)*	1.69 (0.93−3.57)	2.56 (1.49−5.33)**	1.60 (0.86−3.39)
	Malignant neoplasms of digestive organs	42.73	49.70	11.99	44.83	61.79	37.72	4.14 (1.63−16.30)**	3.74 (1.28−15.70)	5.15 (1.87−21.10)**	3.15 (1.00−13.60)
<65 years	Major causes of death	94.45	96.77	85.02	85.94	111.83	88.30	1.14 (0.84−1.64)	1.01 (0.68−1.55)	1.32 (0.92−1.95)	1.04 (0.69−1.60)
	Heart diseases	29.36	31.08	22.04	27.81	33.05	32.07	1.41 (0.81−3.26)	1.26 (0.60−2.98)	1.50 (0.77−3.52)	1.46 (0.70−3.45)
	Ischemic heart diseases	24.78	25.94	19.97	24.45	24.09	30.48	1.30 (0.73−3.23)	1.22 (0.55−3.08)	1.21 (0.57−3.02)	1.53 (0.71−3.86)
	Cerebrovascular diseases	18.82	16.8	27.88	18.89	18.38	12.52	0.60 (0.33−1.29)	0.68 (0.30−1.55)	0.66 (0.30−1.50)	0.45 (0.15−1.11)
	Cerebral infarction	6.61	4.77	14.73	5.86	3.92	4.70	0.32 (0.12−1.02)	0.40 (0.06−1.55)	0.27 (0.00−1.07)	0.32 (0.00−1.29)
	Malignant neoplasms	46.26	48.90	35.11	39.23	60.40	43.71	1.39 (0.87−2.55)	1.12 (0.61−2.21)	1.72 (1.01−3.30)	1.24 (0.67−2.49)
	Malignant neoplasms of digestive organs	24.56	27.21	12.99	25.69	32.70	21.03	2.09 (1.04−6.90)	1.98 (0.83−7.32)	2.52 (1.14−9.23)	1.62 (0.63−5.94)

Continued

Variable	Causes of death	$ASMR_{Total}$ (per 100,000)	$ASMR_{Endemic\ areas}$ (per 100,000)	$ASMR_{Non-endemic\ areas}$ (per 100,000)	$ASMR_{Mild\ endemic\ areas}$ (per 100,000)	$ASMR_{Moderate\ endemic\ areas}$ (per 100,000)	$ASMR_{Severe\ endemic\ areas}$ (per 100,000)	$RR_{Endemic\ areas\ vs.\ Non-endemic\ areas}$	$RR_{Mild\ endemic\ areas\ vs.\ Non-endemic\ areas}$	$RR_{Moderate\ endemic\ areas\ vs.\ Non-endemic\ areas}$	$RR_{Severe\ endemic\ areas\ vs.\ Non-endemic\ areas}$
≥65 years	Major causes of death	321.85	334.21	271.34	318.77	396.92	268.07	1.23 (1.01−1.54)	1.17 (0.93−1.50)	1.46 (1.18−1.84)**	0.99 (0.77−1.28)
	Heart diseases	155.80	171.42	90.74	158.21	191.34	158.17	1.89 (1.36−2.81)***	1.74 (1.20−2.70)*	2.11 (1.48−3.19)***	1.74 (1.18−2.66)*
	Ischemic heart diseases	144.34	161.16	74.42	152.20	173.32	154.70	2.17 (1.52−3.39)***	2.05 (1.37−3.29)**	2.33 (1.60−3.75)***	2.08 (1.38−3.36)**
	Cerebrovascular diseases	79.29	71.38	113.99	68.49	92.49	48.93	0.63 (0.46−0.90)	0.60 (0.39−0.93)	0.81 (0.57−1.20)	0.43 (0.26−0.68)**
	Cerebral infarction	52.88	45.96	83.72	43.25	65.10	24.35	0.55 (0.37−0.86)	0.52 (0.30−0.88)	0.78 (0.49−1.24)	0.29 (0.14−0.53)***
	Malignant neoplasms	86.76	91.41	66.62	92.08	113.10	60.98	1.37 (0.97−2.12)	1.38 (0.90−2.20)	1.70 (1.14−2.66)	0.92 (0.57−1.50)
	Malignant neoplasms of digestive organs	40.45	42.38	31.57	43.39	53.91	25.68	1.34 (0.81−2.61)	1.37 (0.75−2.87)	1.71 (0.97−3.39)	0.81 (0.39−1.75)
Developed regions	Major causes of death	439.69	454.87	361.65	434.75	604.25	314.52	1.26 (0.99−1.67)	1.20 (0.90−1.63)	1.67 (1.29 2.23)***	0.87 (0.65−1.19)
	Heart diseases	211.04	232.11	92.92	210.72	302.28	179.16	2.50 (1.62−4.49)***	2.27 (1.37−4.19)*	3.25 (2.09−5.96)***	1.93 (1.20−3.52)*
	Ischemic heart diseases	192.16	213.79	71.22	205.54	261.57	176.59	3.00 (1.90−5.93)***	2.89 (1.68−5.74)***	3.67 (2.24−7.20)***	2.48 (1.48−4.87)**
	Cerebrovascular diseases	98.89	83.83	187.77	101.19	114.49	38.52	0.45 (0.31−0.69)***	0.54 (0.32−0.90)	0.61 (0.40−0.97)	0.21 (0.10−0.37)***
	Cerebral infarction	56.78	43.38	136.72	54.36	70.44	6.84	0.32 (0.20−0.55)***	0.40 (0.20−0.75)*	0.54 (0.32−0.90)	0.61 (0.40−0.97)*
	Malignant neoplasms	129.76	138.93	80.96	122.84	187.48	96.85	1.72 (1.11−3.12)	1.52 (0.89−2.83)	2.32 (1.45−4.24)**	1.20 (0.71−2.24)
	Malignant neoplasms of digestive organs	69.51	74.54	43.77	70.71	103.20	45.47	1.70 (0.95−4.23)	1.62 (0.78−4.19)	2.36 (1.27−5.77)*	1.04 (0.48−2.71)

Continued

Variable	Causes of death	$ASMR_{Total}$ (per 100,000)	$ASMR_{Endemic\ areas}$ (per 100,000)	$ASMR_{Non\text{-}endemic\ areas}$ (per 100,000)	$ASMR_{Mild\ endemic\ areas}$ (per 100,000)	$ASMR_{Moderate\ endemic\ areas}$ (per 100,000)	$ASMR_{Severe\ endemic\ areas}$ (per 100,000)	$RR_{Endemic\ areas\ vs.\ Non\text{-}endemic\ areas}$	$RR_{Mild\ endemic\ areas\ vs.\ Non\text{-}endemic\ areas}$	$RR_{Moderate\ endemic\ areas\ vs.\ Non\text{-}endemic\ areas}$	$RR_{Severe\ endemic\ areas\ vs.\ Non\text{-}endemic\ areas}$
Under-developed regions	Major causes of death	387.98	396.59	363.73	375.73	381.98	488.63	1.09 (0.87−1.42)	1.03 (0.79−1.39)	1.05 (0.79−1.40)	1.34 (0.96−1.85)
	Heart diseases	152.92	159.81	133.58	163.59	129.51	229.73	1.20 (0.80−1.92)	1.22 (0.78−2.04)	0.97 (0.59−1.64)	1.72 (0.99−3.02)
	Ischemic heart diseases	140.20	148.31	115.60	149.52	122.17	215.91	1.28 (0.85−2.15)	1.29 (0.81−2.25)	1.06 (0.63−1.85)	1.87 (1.04−3.39)
	Cerebrovascular diseases	97.02	94.52	105.58	73.93	102.52	130.82	0.90 (0.59−1.50)	0.70 (0.38−1.28)	0.97 (0.57−1.70)	1.24 (0.64−2.30)
	Cerebral infarction	63.09	61.56	66.69	43.70	62.46	93.68	0.92 (0.54−1.80)	0.66 (0.30−1.43)	0.94 (0.47−1.94)	1.40 (0.62−3.03)
	Malignant neoplasms	138.04	142.26	124.57	138.20	149.96	128.07	1.14 (0.78−1.79)	1.11 (0.71−1.84)	1.20 (0.76−2.00)	1.03 (0.59−1.77)
	Malignant neoplasms of digestive organs	59.00	62.42	46.28	67.17	56.26	58.22	1.35 (0.75−3.09)	1.45 (0.73−3.45)	1.22 (0.55−3.02)	1.26 (0.48−3.22)

Note: * $P<0.05$; ** $P<0.01$; *** $P<0.001$ (adjusted).

Abbreviation: ASMR=age-standardized mortality rate; *RR*=rate ratio.

Preplanned Studies

Machine Learning-Based Assessment of Heat Vulnerability at County-Level — China, 2020

Yirong Liu[1]; Yuanyuan Liu[1]; Runmei Ma[1]; Qing Wang[1]; Tiantian Li[1,#]

Summary

What is already known about this topic?

Heat-vulnerability assessment is an essential approach for identifying populations and regions that are vulnerable to extreme heat and supporting targeted climate adaptation and public-health interventions.

What is added by this report?

This study updates the national assessment to 2020; the Boruta algorithm is employed to objectively identify the indicators most strongly associated with the proportion of non-accidental deaths on extreme heat days and a revised heat-vulnerability index (HVI) is constructed.

What are the implications for public health practice?

The updated county-level HVI provides policymakers with a precise understanding of current heat-vulnerability patterns in China. These findings will facilitate a more effective identification of high-vulnerability regions.

ABSTRACT

Introduction: Extreme heat poses an increasing threat to public health. This study evaluates the county-level heat vulnerability across China in 2020.

Methods: A comprehensive county-level assessment of heat vulnerability was conducted across China using the 2020 data encompassing socioeconomic, demographic, environmental, and infrastructure-related indicators. The Boruta machine-learning algorithm was applied to objectively identify indicators associated with the proportion of non-accidental deaths on extreme-heat days. A heat-vulnerability index (HVI) was constructed using principal component analysis and validated using linear regression against the proportion of non-accidental deaths on extreme-heat days.

Results: Ten key indicators were integrated into a county-level HVI representing national heat-vulnerability patterns in 2020. The HVI demonstrated a significant positive correlation with the proportion of non-accidental deaths on extreme-heat days (P<0.05). Spatial analysis revealed that high-vulnerability counties were primarily concentrated in Southwestern China, whereas low-vulnerability areas were mainly located in South China and the eastern coastal regions.

Conclusion: This study delivers an accurate and up-to-date representation of current vulnerability patterns by providing an updated and refined county-level assessment for 2020, supporting evidence-based public-health planning, efficient resource allocation, and climate-adaptation strategies to mitigate the impact of extreme heat.

Extreme-heat exposure has been consistently associated with increased morbidity and mortality (*1*). Considering the substantial regional and population heterogeneity of heat-related impacts, assessing vulnerability and identifying vulnerable regions are essential for climate-change adaptation (*2*). The multi-indicator heat-vulnerability index (HVI) is widely used for such assessments and is developed in three steps: vulnerability-indicator selection, assigning of indicator weights, and composite-index calculation (*3*–*4*). However, most existing studies select indicators based on a literature review or expert judgment, which introduces subjectivity and lacks quantitative validation. This may lead to the inclusion of weakly related indicators and omission of key determinants, thereby compromising the accuracy and reliability of the HVI. In China, the current heat-vulnerability assessments share these limitations, and county-level evaluations remain scarce. The only national county-level study reflects the conditions in 2010 and no longer represents the current spatial distribution of heat vulnerability. Therefore, this study applies a machine-learning approach for objective indicator screening, and uses the most recently available data to construct a county-level HVI for China for 2020. This

can be used to identify highly vulnerable regions and inform targeted public health and climate-adaptation strategies. The year 2020 was selected because the Seventh National Population Census provides the most comprehensive and up-to-date county-level demographic data required for the vulnerability assessment.

Following the framework of the Intergovernmental Panel on Climate Change, heat vulnerability was assessed across two dimensions: sensitivity and adaptive capacity (*5*). The methodology applied in this study included the following steps: indicator screening using the Boruta algorithm, HVI calculation using principal component analysis (PCA), and HVI validation.

This study first compiled demographic, socioeconomic, and land-use variables for 2,844 counties nationwide (including urban districts, county-level cities, counties, and autonomous counties) and then extracted 323 counties with complete daily non-accidental death data and daily maximum-temperature records. Data from these 323 counties were used to screen for HVI indicators to ensure that they were objective and strongly associated with the proportion of nonaccidental deaths on extreme-heat days. Boruta analysis was conducted using indicators from these counties as input variables and the proportion of non-accidental deaths on extreme-heat days as the outcome. The proportion is defined as the number of non-accidental deaths on extreme-heat days divided by the total number of non-accidental deaths during the warm season (May–October). Extreme-heat days were defined as days on which the daily maximum temperature exceeded the 95th percentile of the county-specific historical maximum-temperature distribution during the warm season from 2013 to 2018. Boruta, a feature-selection algorithm based on random forests, constructs randomly permuted "shadow features" and compares their importance with that of the original variables. Through iterative statistical testing, Boruta identifies all features that exhibit a significant association with the outcome, thereby reducing the subjectivity in the indicator selection. Notably, the 323 counties used for indicator screening and vulnerability validation span all seven major geographical regions of China, covering diverse climatic and socioeconomic contexts. The selected indicators were applied uniformly to 2,844 county-level units to construct the national HVI. The HVI construction involved three main steps: indicator normalization, dimensionality reduction, and composite-index calculation. First, all retained indicators were normalized to remove the influence of different units. Second, PCA was conducted to address the multicollinearity among the variables and reduce redundancy across the indicator categories. The proportion of total variance explained by each principal component (PC) was obtained from the PCA output. PC scores were classified into six ordered categories (1–6) based on standard deviation (SD) intervals from the mean to enhance interpretability and mitigate the influence of extreme values: ≥2 SD below the mean, 1–2 SD below the mean (includes 1 SD below, excludes 2 SD below), 0–1 SD below the mean [includes the mean (0 SD), excludes 1 SD below], 0–1 SD above the mean [excludes the mean (0 SD), includes 1 SD above], 1–2 SD above the mean (excludes 1 SD above, includes 2 SD above), and >2 SD above the mean. Owing to the lack of clear empirical evidence on the relative influence of each PC on heat vulnerability, and to avoid subjective bias while ensuring simplicity and reproducibility in index construction, equal weights were assigned to all retained PCs, and their scores were summed to generate the HVI for each county (*6*). Finally, linear regression was performed to evaluate the HVI reliability using the proportion of non-accidental deaths on extreme-heat days as the dependent variable and HVI as the independent variable. Demographic data were obtained from the China Population Census Yearbook 2020; gross domestic product (GDP) data were sourced from the 2021 China County Statistical Yearbook and statistical bulletins of districts; air conditioning (AC) was estimated using provincial-level data adjusted by urban–rural population composition (Supplementary Material, available at https://weekly.chinacdc.cn/); and land-use data were derived from the Geo-Simulation and Optimization System platform (Supplementary Table S1, available at https://weekly.chinacdc.cn/) (*7*). Daily non-accidental deaths were provided by the China CDC, and daily maximum-temperature data were obtained from the European Centre for Medium-Range Weather Forecasts (ECMWF) (Supplementary Table S2, available at https://weekly.chinacdc.cn/). All data processing and analyses were performed using R software (version 4.4.1; R Core Team, Vienna, Austria) and ArcGIS (version 10.8; Esri, Redlands, CA, USA).

As shown in Figure 1, we identified 10 key indicators that were significantly associated with the proportion of non-accidental deaths on extreme-heat days. These included AC, population density, aged ≥ 65 years and ≤5 years, illiteracy ratio, proportion of

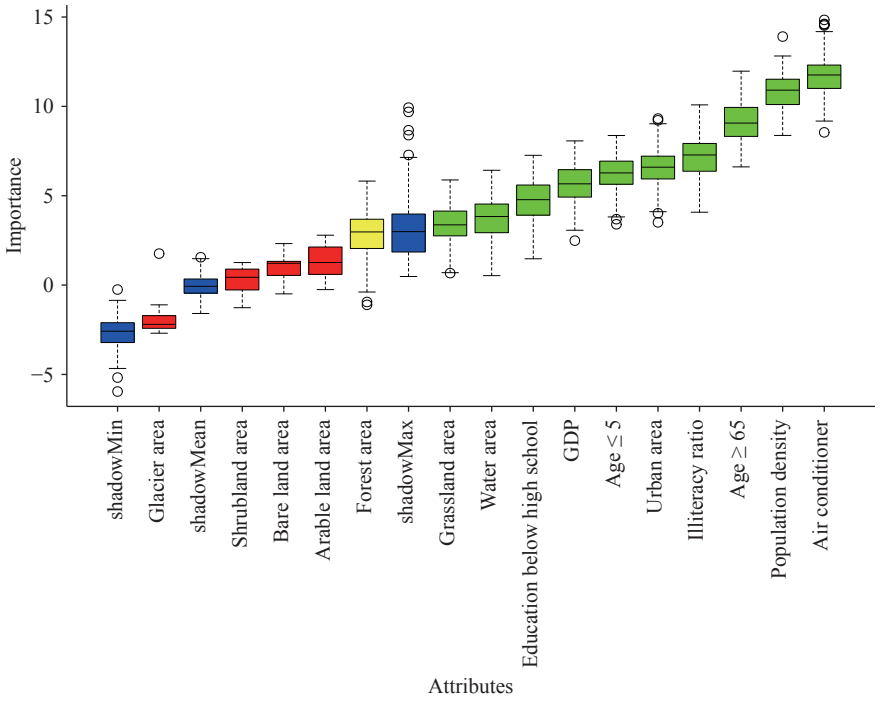

FIGURE 1. Ranking of heat-vulnerability indicators screen (*N*=323).
Note: Green indicates features with importance significantly higher than the shadow features and are thus retained; yellow indicates features with importance comparable to the shadow features and require further iterative assessment; blue represents the shadow features; red indicates features with importance lower than the shadow features and are thus removed.
Abbreviation: GDP=gross domestic product.

education below senior high school, GDP, and proportions of urban, water, and grassland areas.

Supplementary Figure S1 (available at https://weekly.chinacdc.cn/) shows a scree plot used to determine the number of PCs. We selected PCs with eigenvalues greater than 1, and four PCs were extracted, which cumulatively explained 76% of the variance in the original 10 variables (Table 1). PC1 represented the residential environment and resource allocation, characterized by high loadings on AC, population density, and grassland. PC2 reflected population structure and social vulnerability, comprising ages ≤5 and ≥65 years, as well as the illiteracy ratio. PC3 captured educational-attainment and urban-development levels, represented by the proportion of people who were educated below senior high school and in urban areas. PC4 was dominated by water-body proportion, indicating local hydrological features.

Supplementary Figure S2 (available at https://weekly.chinacdc.cn/) shows a frequency distribution of HVI. The spatial analysis revealed pronounced regional variations in heat vulnerability across China (Figure 2). Counties with high vulnerability were primarily concentrated in Southwestern China, including Yunnan, Guangxi, Sichuan, Guizhou, and Tibet, whereas low-vulnerability areas were mainly distributed in South China and the eastern coastal regions. Results from the linear regression analysis, conducted after confirming a clear linear relationship between the HVI and proportion of non-accidental deaths on extreme-heat days, indicated that each one-unit increase in HVI was associated with an average 2.41% increase in the proportion of non-accidental deaths on extreme-heat days (95% confidence interval: 1.05, 3.77%, $P<0.05$).

DISCUSSION

This study comprehensively assessed county-level heat vulnerability across China in 2020 using a machine-learning-based approach and confirmed a significant positive correlation between the HVI and proportion of non-accidental deaths on extreme-heat days. These findings revealed pronounced spatial disparities in heat vulnerability nationwide.

A major methodological contribution of this study is the integration of machine learning into indicator selection. Using the Boruta algorithm, the 10 indicators most strongly associated with the proportion

TABLE 1. Factor loadings of the heat-vulnerability indicators in Chinese counties (*N*=2,844).

Indicators	PC1	PC2	PC3	PC4
Air conditioner (sets per 100 households)	0.79*	0.14	0.05	0.20
Population density (persons/km^2)	−0.77*	0.05	−0.39	−0.09
Age ratio (age ≤5) (%)	−0.14	0.88*	0.17	0.13
Age ratio (age ≥65) (%)	−0.24	−0.78*	0.27	−0.09
Illiteracy ratio (%)	0.32	0.72*	0.28	−0.16
Education below high school (%)	0	0.07	0.88*	0.07
Urban area (%)	0.20	0.04	0.78*	0
GDP (10,000 CNY)	0.60	−0.03	0.56	0.78*
Grassland area (%)	−0.70*	−0.43	0.10	0.16
Water area (%)	0.15	0.06	0.09	0.93*

Abbreviation: GDP=gross domestic product; PC=principal component; CNY=Chinese Yuan.
* Absolute values ≥0.7 are the most significant loadings on that factor.

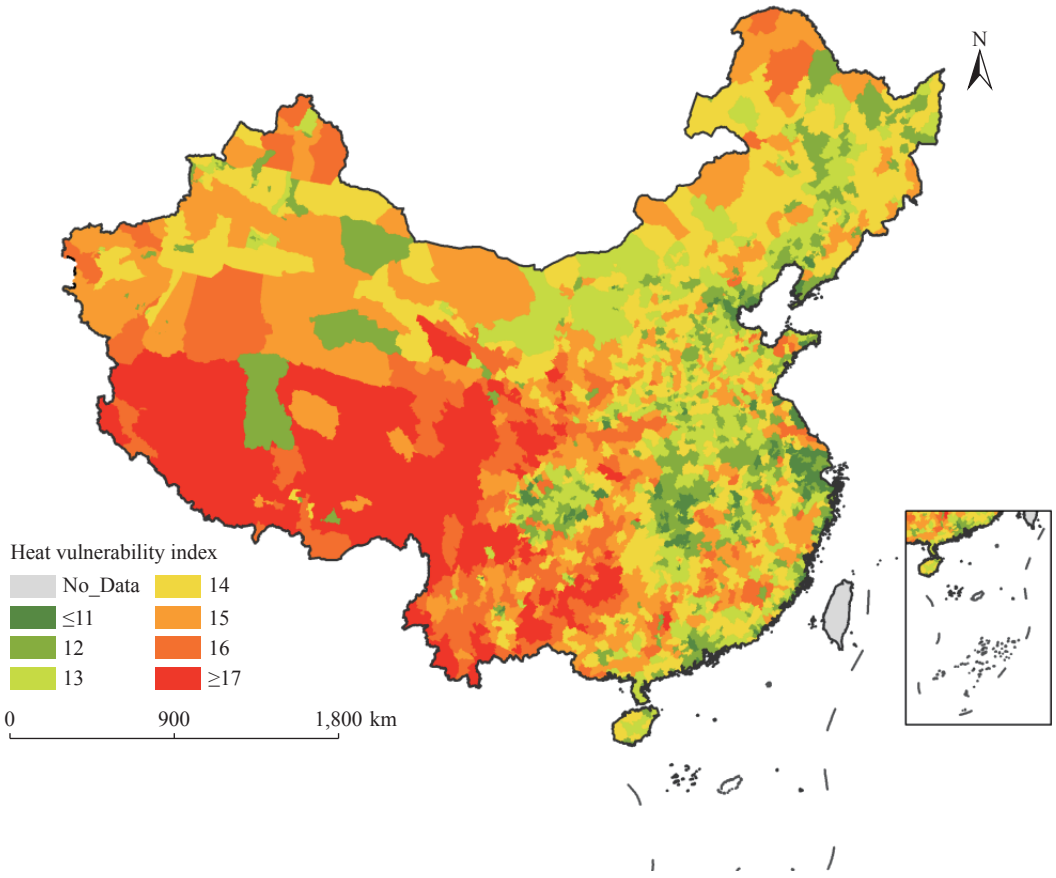

FIGURE 2. Spatial distribution of heat vulnerability in counties of China in 2020 (*N*=2,844).
Map approval number: GS 京 (2026)0497 号.

of non-accidental deaths on extreme-heat days were objectively identified. This overcame the subjectivity of the literature or expert-based selection and enhanced the scientific rigor and robustness of the HVI by avoiding weakly correlated variables (*8*). These indicators reflect multiple dimensions of population characteristics, socioeconomic conditions, and environmental features. Therefore, these indicators not only help explain the underlying mechanisms driving regional differences in heat vulnerability but also provide clear public health and heat adaptation implications. For regions with higher vulnerability,

more targeted public health preparedness, greater protection of sensitive populations, strengthened social support, and environmental resilience may be required.

Southwestern China has been consistently identified as a region with persistently high heat vulnerability, which is consistent with earlier research (*9*). This consistency underscores the stability of vulnerability patterns in this region over the past decade, suggesting that Southwestern China should remain a focal area for heat-related health prevention and adaptation. Moreover, the results highlight the dynamic nature of heat vulnerability across China. Vulnerability has increased significantly in several south-central regions, whereas some northern areas have experienced a decline. These spatiotemporal shifts indicate that heat vulnerability is not static but evolves in response to climate change, socioeconomic development, and policy-driven adaptation measures (*10*).

This study had several limitations. First, the HVI was constructed using 2020 indicator data, whereas mortality and meteorological data were from 2013 to 2018, creating a temporal mismatch that may bias the indicator selection and affect the consistency between the HVI and mortality validation. To reduce this bias, six years of daily non-accidental deaths were aggregated to calculate the proportion of deaths on extreme heat days, which smoothed interannual fluctuations and provided a more stable estimate than the single-year data. Additionally, owing to data constraints, county-level AC was estimated using provincial urban–rural AC data combined with county-level population structures. This derived measure may introduce uncertainty and cannot fully reflect true county-level AC levels; however, it represents the most feasible and reasonable approach under the current data conditions. Finally, an equal-weighting method was adopted to aggregate all the retained PCs, which did not fully consider the actual relative importance of each component to heat vulnerability. In future research, more refined weighting strategies, such as regression coefficient-based weighting, Bayesian hierarchical models, and data-driven machine-learning approaches, may be explored to further optimize index construction.

In conclusion, this study refined the heat-vulnerability-assessment framework by incorporating machine learning techniques and provided an updated county-level HVI for China in 2020. The findings revealed substantial spatial heterogeneity, with Southwestern China exhibiting a significantly higher vulnerability than the southern and eastern coastal regions. These results offer an accurate understanding of current vulnerability patterns and provide a scientific foundation for public health planning, targeted resource allocation, and climate-adaptation strategies to mitigate the health impacts of extreme heat.

Conflicts of interest: No conflict of interest.

Acknowledgments: This study was supported by the Capital's Funds for Health Improvement and Research (grant number 2024-1G-4231).

Ethical statements: The mortality dataset used in this study was approved by the Ethical Review Committee of the National Institute of Environmental Health, Chinese Center for Disease Control and Prevention (Approval No. 202102).

Funding: Supported by the Capital's Funds for Health Improvement and Research (grant number 2024-1G-4231, TL).

doi: 10.46234/ccdcw2026.067

Corresponding author: Tiantian Li, litiantian@nieh.chinacdc.cn.

[1] National Key Laboratory of Intelligent Tracking and Forecasting for Infectious Diseases, China CDC Key Laboratory of Environment and Population Health, National Institute of Environmental Health, Chinese Center for Disease Control and Prevention & Chinese Academy of Preventive Medicine, Beijing, China.

Submitted: December 05, 2025
Accepted: February 28, 2026
Issued: April 03, 2026

REFERENCES

1. Liu JW, Varghese BM, Hansen A, Xiang JJ, Zhang Y, Dear K, et al. Is there an association between hot weather and poor mental health outcomes? A systematic review and meta-analysis. Environ Int 2021;153:106533. https://doi.org/10.1016/j.envint.2021.106533.
2. Zhao Q, Guo YM, Ye TT, Gasparrini A, Tong SL, Overcenco A, et al. Global, regional, and national burden of mortality associated with non-optimal ambient temperatures from 2000 to 2019: a three-stage modelling study. Lancet Planet Health 2021;5(7):e415 – 25. https://doi.org/10.1016/S2542-5196(21)00081-4.
3. Bradford K, Abrahams L, Hegglin M, Klima K. A heat vulnerability index and adaptation solutions for Pittsburgh, Pennsylvania. Environ Sci Technol 2015;49(19):11303 – 11. https://doi.org/10.1021/acs.est.5b03127.
4. Fall S, Coulibaly K, Quansah J, El Afandi G. Differential urban heat vulnerability: the tale of three Alabama cities. Urban Sci 2023;7(4):121. https://doi.org/10.3390/urbansci7040121.
5. Solomon S, Qin D, Manning M, Chen Z, Marquis M, Averyt KB, et al. Climate change 2007: the physical science basis: contribution of working group I to the fourth assessment report of the intergovernmental panel on climate change. Cambridge: Cambridge University Press, United Kingdom and New York, NY, USA, 996 pp. https://www.ipcc.ch/site/assets/uploads/2018/05/ar4_wg1_full_report-1.pdf.

6. Reid CE, O'Neill MS, Gronlund CJ, Brines SJ, Brown DG, Diez-Roux AV, et al. Mapping community determinants of heat vulnerability. Environ Health Perspect 2009;117(11):1730 – 6. https://doi.org/10.1289/ehp.0900683.
7. Luo M, Hu GH, Chen GZ, Liu XJ, Hou HY, Li X. 1 km land use/land cover change of China under comprehensive socioeconomic and climate scenarios for 2020-2100. Sci Data 2022;9(1):110. https://doi.org/10.1038/s41597-022-01204-w.
8. Grigorescu I, Mocanu I, Mitrică B, Dumitrașcu M, Dumitrică C, Dragotă CS. Socio-economic and environmental vulnerability to heat-related phenomena in Bucharest metropolitan area. Environ Res 2021;192:110268. https://doi.org/10.1016/j.envres.2020.110268.
9. Wang Q, Zhang YY, Ban J, Zhu HH, Xu HY, Li TT. The relationship between population heat vulnerability and urbanization levels: a county-level modeling study across China. Environ Int 2021;156:106742. https://doi.org/10.1016/j.envint.2021.106742.
10. Wu Y, Wen B, Ye TT, Huang WZ, Liu YM, Gasparrini A, et al. Estimating the urban heat-related mortality burden due to greenness: a global modelling study. Lancet Planetary Health 2025;9(7):101235. https://doi.org/10.1016/S2542-5196(25)00062-2.

SUPPLEMENTARY MATERIALS

SUPPLEMENTARY TABLE S1. Basic information on all indicator data (*N*=2,844).

Indicators	Definition	Year	Spatial scale	Data source	Data handling
Population density (people/km^2)	The per-km^2 population size in each county	2020	County-level	The Seventh National Population Census (2020)	/
Illiteracy ratio (%)	Proportion of illiterate individuals among the population aged ≥15 years (%)				
Age ratio (age ≤ 5) (%)	Proportion of individuals aged under 5 years (%)				
Age ratio (age ≥ 65) (%)	Proportion of individuals aged ≥65 years (%)				
Education below high school (%)	Proportion of individuals aged ≥6 years with education lower than high school (%)				
GDP (10,000 CNY)	Gross domestic product	2020	County-level	China County Statistical Yearbook (Township & County Volume) 2021, and statistical bulletins of urban districts	/
AC	Air-conditioner ownership per 100 households	2020	31 provinces	China Statistical Yearbook 2021	Converted to county-level using Equation (1).
Land use/land cover (%)	Including cropland, forest, bare land, grassland, water, urban area, shrubland, and ice/snow	2020	1 km × 1 km	Geographical Simulation and Optimization System (GeoSOS) http://www.geosimulation.cn/China_SSP-RCP_1km.html	To harmonize all raster datasets with a spatial resolution of 1 km to the county-level, we aggregated the grids using ArcGIS zonal statistics. Each county boundary was treated as a zonal unit, and all 1-km raster cells within the zone were summarized based on the variable type to produce county-level indicators.

Note: The land use/land cover dataset was developed by Luo et al. and provides a 1-km resolution land-use/land-cover dataset for China for 2020–2100 across 24 SSP-RCP scenario combinations (including five SSP baseline scenarios). It includes eight land-use types: urban, cropland, forest, grassland, shrubland, water, bare land, and ice/snow, and is publicly available in the GeoTIFF format. The dataset has been validated through multiple approaches and calibrated against the 2010 European Space Agency Climate Change Initiative observations, achieving an overall accuracy of 0.82 and a Kappa coefficient of 0.66, with area deviations for major land types controlled within ±5%. In this study, we specifically used the 2020 data under the "SSP2 Baseline" scenario. Although different SSP scenarios show some minor variations in 2020, the spatial patterns of key land classes (e.g., cropland, forest, and urban land) remain highly consistent across scenarios; thus, selecting any scenario for the baseline year does not materially affect the main results. The SSP2 Baseline scenario, which assumes conventional socioeconomic development, best reflects China's actual development conditions in 2020 and provides a realistic representation of land-use patterns for the base year.
Abbreviation: CNY=Chinese Yuan.

Air-conditioning Factor in Each County

The conversion of the provincial air-conditioner ownership per 100 households to county data:

$$AC = AC_R \times POP_R + AC_U \times POP_U \quad (1)$$

AC: Air-conditioner ownership per 100 households
AC_R: Air-conditioner ownership per 100 rural households
POP_R: Proportion of rural population
AC_U: Air-conditioner ownership per 100 urban households
POP_U: Proportion of urban population

SUPPLEMENTARY TABLE S2. Basic information on non-accidental deaths and meteorological data (*N*=323).

Variables	Year	Temporal resolution	Spatial resolution	Source	Data description and preprocessing
Maximum temperature	2013–2018	hourly	0.1°×0.1°	ECMWF https://cds.climate.copernicus.eu/	The data were spatially aggregated at the county level by first extracting all grid cells within the administrative boundaries of each county, calculating the daily maximum temperature for each grid cell from hourly data, and then averaging these values to obtain a county-level daily maximum temperature time series.
Non-accidental deaths	2013–2018	daily	323 counties (including urban districts, county-level cities, counties)	China CDC	The mortality data were obtained from the China CDC via the Chinese Environmental Public Health Tracking and Risk Assessment Platform. Counties were included in the analysis if they met the following conditions: 1) participation in the national mortality surveillance network of the China CDC or the existence of a standardized local death-registration system; 2) an average annual mortality rate greater than 4.5‰; 3) stable temporal patterns in mortality reporting over the study period; and 4) year-to-year variability in mortality rates below 20%. The final dataset covered approximately 222 million residents across seven major geographical regions of China and comprised approximately 6.36 million registered deaths, among which 5.93 million were classified as non-accidental. Ethical approval for the use of these data was granted by the Ethical Review Committee of the National Institute of Environmental Health, Chinese Center for Disease Control and Prevention (approval number: 202102).

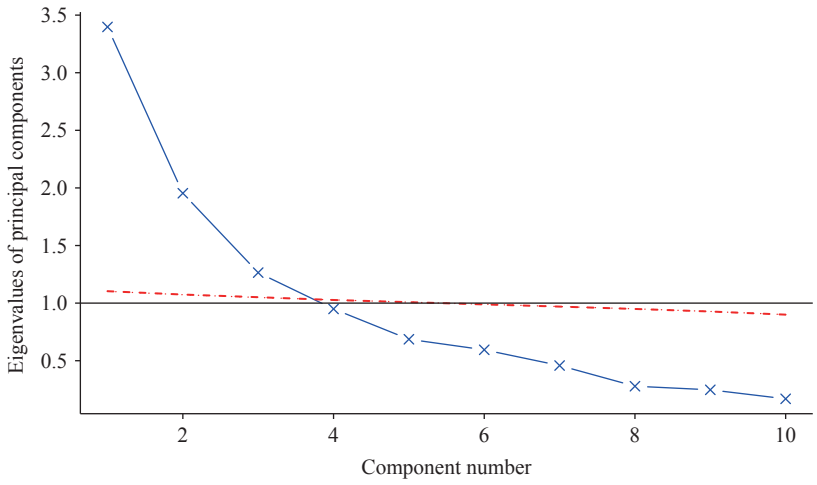

SUPPLEMENTARY FIGURE S1. Scree plot with parallel analysis for determining the number of retained principal components.
Note: The blue lines represent the actual eigenvalues of each principal component, the red dashed lines denote the eigenvalue reference lines derived from parallel analysis, and the horizontal line is the reference line corresponding to an eigenvalue of 1.

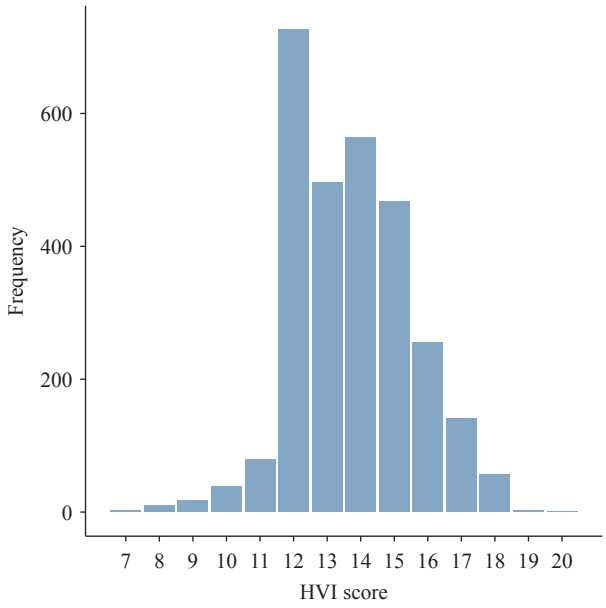

SUPPLEMENTARY FIGURE S2. Frequency distribution of HVI in China.
Abbreviation: HVI=heat vulnerability index.

Preplanned Studies

Analysis of Indoor Radon Concentrations in Urban and Rural Areas in 20 Cities — China, 2023–2025

Bowei Ding[1]; Yunyun Wu[1,#]; Xianliang Wang[2,#]; Yanchao Song[1]; Hang Du[2]; Haoran Sun[1]; Jialu Li[1]; Changsong Hou[1]

Summary

What is already known about this topic?

Indoor radon is the second leading cause of lung cancer after smoking, but previous studies in China have mainly focused on urban areas, with limited data from rural areas.

What is added by this report?

A survey of 20 cities from 2023–2025 shows that median indoor radon concentrations in rural areas (72 Bq/m3) are higher than in urban areas (65 Bq/m3). Higher levels are also associated with northern regions, low floor levels, brick-wood structures, and energy-efficient buildings.

What are the implications for public health practice?

It is recommended to control radon release from building materials at the source, improve ventilation, seal cracks in walls and floors, and pay attention to rural and cold climate regions.

ABSTRACT

Introduction: As public concern over indoor environmental quality and healthy living conditions continues to grow, understanding indoor radon levels, their determinants, and urban-rural disparities in residential buildings has become increasingly important.

Methods: This study measured indoor radon concentrations in 1,139 dwellings across 20 cities from 2023 to 2025 using the solid-state nuclear track detector (SSNTD) technique over a 6-month cumulative sampling period.

Results: The median indoor radon concentration was 67 Bq/m^3, corresponding to an annual effective dose of 2.03 mSv/year. Urban areas had a median concentration of 65 Bq/m^3 (dose: 1.97 mSv/year), while rural areas reached 72 Bq/m^3 (dose: 2.18 mSv/year).

Conclusion: Comparison with previous data revealed an increasing trend in indoor radon concentrations nationwide, with rural areas exhibiting significantly higher levels than urban areas. To mitigate indoor radon pollution, a comprehensive strategy is recommended, including controlling radon exhalation from building materials at the source, ensuring adequate ventilation, and inspecting and sealing structural cracks.

Ionizing radiation poses well-documented health risks, and radon (^{222}Rn) constitutes the most significant source of natural ionizing radiation exposure (*1*). This radioactive gas originates from uranium decay in soil, rocks, and building materials, entering indoor environments through diffusion and advection. The World Health Organization identifies indoor radon as the second leading cause of lung cancer after smoking (*1*). Epidemiological studies in Europe (*2*), North America (*3*), and China (*4*) provide compelling evidence linking indoor radon exposure to lung cancer risk, even at the relatively low concentrations typical of residential buildings (*1*). Understanding indoor radon concentrations and their determinants is therefore essential for developing evidence-based building design standards and improving public health outcomes. However, most previous indoor radon surveys in China focused predominantly on urban areas, leaving rural radon exposure data limited. As of 2021, China's rural permanent population stood at 509.78 million, and the potential health implications for this substantial population underscore the need for further investigation into rural indoor radon levels. This study represents the largest and most comprehensive indoor radon survey conducted in China in recent years, systematically measuring radon concentrations in urban and rural dwellings across 20 cities from 2023 to 2025. A detailed questionnaire capturing potential influencing factors accompanied each measurement. By integrating measurement data with questionnaire

responses, this study aimed to compare radon levels between urban and rural areas, identify key factors influencing indoor radon concentrations, and provide a scientific basis for developing effective radon control and mitigation measures.

This study adopted a combination of stratified sampling and purposive selection. Cities were chosen to represent diverse climatic zones and geographical regions, with approximately 40 urban and 20 rural dwellings selected per city to reflect typical local building types. Surveys spanned from July 2023 to July 2025, with each city undergoing approximately six months of long-term cumulative monitoring that covered the winter season. Indoor radon concentrations were measured using the solid-state nuclear track detector (SSNTD) technique for long-term cumulative assessment. The study employed LIH radon detectors manufactured by the National Institute for Radiological Protection (NIRP) in China, with CR-39 (Fukuvi Chemical Industry Co., Ltd., Fukui, Japan) as the detecting material. After sampling, detectors were placed in containers filled with 6.25 mol/L NaOH and etched in a water bath at 80 °C for 8 hours. Etching rendered latent tracks clearly visible under microscopic examination. Average indoor radon concentrations were then calculated from the observed track density, exposure duration, and a calibration factor of 4.8 Tr/cm^2 per Bq/(h·m^3), as determined through standard procedures of the National Institute of Metrology, China.

Indoor radon concentration in air was calculated using Equation (1):

$$C_{Rn} = \frac{n - n_b}{t \cdot F} \quad (1)$$

Where: C_{Rn} — average indoor radon concentration during the exposure period, Bq/m^3; n — track density, Tr/cm^2; n_b — background track density, Tr/cm^2; t — sampling time, h; F — calibration factor, (Tr/cm^2) / [Bq/(h·m^3]].

The annual effective dose from indoor radon exposure was estimated using the equation recommended by the United Nations Scientific Committee on the Effects of Atomic Radiation (UNSCEAR) (*5*), as shown in Equation (2):

$$E = C_{R_n} \cdot F \cdot T \cdot DCF \quad (2)$$

Where: E — effective dose (mSv/year); C_{Rn} — indoor radon concentration (Bq/m^3); F — equilibrium factor between radon and its progeny, 0.48 (*6*); T — exposure time, 7,000 h/year; DCF — dose conversion factor, 9 nSv/[(Bq·h)/m^3] (*7*).

Statistical analyses were conducted using R (version 4.5.0; R Foundation for Statistical Computing, Vienna, Austria). Two-group comparisons employed Student's t-test or the Mann-Whitney U test, as appropriate, while comparisons among three or more groups used analysis of variance (ANOVA) or the Kruskal-Wallis test. Statistical significance was set at P<0.05.

This survey yielded 1,139 valid indoor radon measurements, with a median concentration of 67 Bq/m^3 (range: 5–587 Bq/m^3). Overall, 24.1% of dwellings exceeded 100 Bq/m^3, and 0.6% exceeded

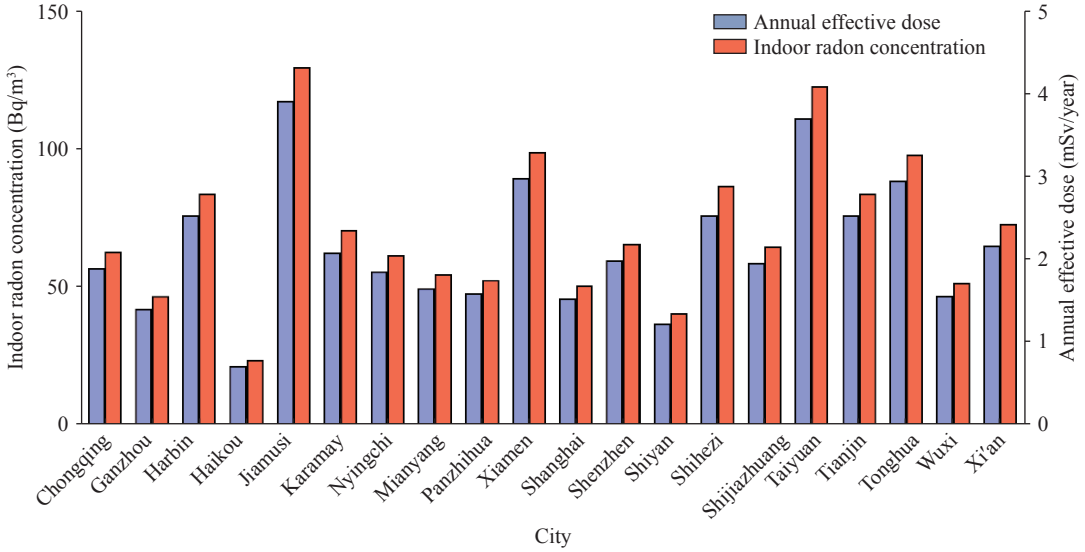

FIGURE 1. Median indoor radon concentrations (Bq/m^3) and annual effective doses (mSv/year) for residents across 20 cities in China.

300 Bq/m^3. Assessing effective doses in residential settings is essential for characterizing indoor radon exposure (*8*). Figure 1 presents the median indoor radon concentrations and corresponding annual effective doses across the 20 cities. Urban areas contributed 810 measurements (median: 65 Bq/m^3; dose: 1.97 mSv/year), with 20.9% exceeding 100 Bq/m^3 and 0.1% exceeding 300 Bq/m^3. Rural areas contributed 329 measurements (median: 72 Bq/m^3; dose: 2.18 mSv/year), with 32.2% exceeding 100 Bq/m^3 and 1.8% exceeding 300 Bq/m^3. Indoor radon concentrations differed significantly between rural and urban areas (P<0.001), with rural levels exceeding urban levels.

Indoor radon concentrations were further analyzed by geographic region, climate zone, floor level, building structure type, and construction period. Northern cities exhibited significantly higher concentrations than southern cities (P<0.001). According to the Uniform Standard for Design of Civil Buildings (GB 50352), China encompasses five climate zones: the severe cold zone (SCZ), cold zone (CZ), hot-summer and cold-winter zone (HCZ), hot-summer and warm-winter zone (HWZ), and mild zone (MZ) (no data available). Concentrations differed significantly among these zones (P<0.001), with higher levels in the SCZ and CZ than in the HCZ and HWZ; concentrations in the HWZ also significantly exceeded those in the HCZ. Floor level similarly influenced radon concentrations (P<0.001), with ground-floor dwellings recording higher levels than upper floors. Building structure type showed significant effects (P<0.05), as brick-wood structures (BWS) exhibited higher concentrations than reinforced concrete structures (RCS) and brick-concrete structures (BCS). Because only the SCZ and CZ contained buildings spanning all three development stages (*9*), construction-period analysis was restricted to these zones, revealing significant differences among building periods (P<0.001). Table 1 presents detailed statistical results.

TABLE 1. Distribution of indoor radon concentrations across different factors.

Influencing factors		Sample	Indoor radon concentration (Bq/m^3)		
			Median (25th–75th)	*Z*/*H*-value	*P*
City	Urban	810	65 (47–93)	−3.567	0.001
	Rural	329	73 (51–116)		
Region	North	521	90 (67–121)	−16.548	0.001
	South	618	53 (41–70)		
Building Climate Zones	SCZ	345	84 (68–116)	266.183	0.001
	CZ	230	89 (59–122)		
	HCZ	403	51 (41–65)		
	HWZ	161	59 (36–95)		
Floor Level	1	237	71 (50–122)	18.333	0.001
	2–3	249	61 (42–90)		
	4–9	409	68 (48–98)		
	≥10	244	68 (51–94)		
Building Structure	RCS	1,009	67 (47–97)	6.173	0.046
	BCS	88	66 (51–103)		
	BWS	42	80 (50–140)		
Building Period	Pre–1980	4	106 (72–110)	29.939	0.001
	1980–1989	23	47 (40–66)		
	1990–1999	59	73 (58–99)		
	2000–2010	155	93 (70–122)		
	Post–2010	171	84 (65–115)		

Note: The *Z*- and *H*-values represent the test statistics for the Mann-Whitney U test and the Kruskal-Wallis test, respectively.
Abbreviation: SCZ=severe cold zone; CZ=cold zone; HCZ=hot-summer and cold-winter zone; HWZ=hot-summer and warm-winter zone; RCS=reinforced concrete structure; BCS=brick-concrete structure; BWS=brick-wood structure.

DISCUSSION

This study characterized indoor radon concentrations in 1,139 dwellings across 20 cities in China from 2023 to 2025. The findings align with previous reviews (*10*–*11*), which documented a continuously rising trend in indoor radon concentrations across China over recent decades. China's Standards for Indoor Air Quality (GB/T 18883-2022) establish a radon reference level of 300 Bq/m^3, representing the maximum acceptable average concentration and serving as a nationally recognized risk benchmark rather than a strict safety threshold. When indoor radon exceeds this level, remedial action is recommended.

Ventilation rate emerged as a critical determinant of indoor radon concentration. During winter months, the substantially lower temperatures in northern regions and cold zones discourage frequent ventilation, promoting indoor radon accumulation. All four cities with radon concentrations exceeding 300 Bq/m^3 are located in northern China. In these high-radon areas, elevated concentrations reflect low ventilation rates, partly attributable to the thicker walls designed to resist cold climates.

Since 1986, China has progressively implemented residential building energy efficiency standards for new urban construction. However, previous studies (*12*–*13*) demonstrated that energy-saving designs inadvertently reduce ventilation rates, thereby promoting indoor radon accumulation. Moreover, incorporating industrial by-products into building materials — while improving energy efficiency — has increased their radium content, consequently elevating indoor radon concentrations (*14*). These findings suggest that current energy efficiency standards may need revision to balance thermal performance with indoor air quality, particularly with respect to radon mitigation.

Unlike modern medium- and high-rise buildings, bungalows experience more direct radon exhalation from the underlying soil. Direct ground-floor contact with the soil enables radon gas to infiltrate indoor spaces more readily, resulting in elevated concentrations (*15*). BCS and BWS are typically used for low-rise buildings in rural areas, whereas RCS predominates in urban high-rise construction. Low-rise buildings face the combined influence of both soil-derived and building-material-derived radon. Furthermore, rural BCS and BWS dwellings tend to be older — 42% were constructed before 2000, compared with only 15% of RCS buildings. In many BCS and BWS dwellings, floors are laid directly on the soil, allowing radon to infiltrate through floor cracks or foundation gaps and elevating indoor concentrations.

Indoor radon levels exceeding the national reference level signal potential public health risks, and effective mitigation demands coordinated interventions at multiple levels. Source control measures should encompass stricter regulation of building materials with high radium content and enforcement of radon exhalation standards. At the building level, improved ventilation, higher air exchange rates, and sealing of structural cracks can limit radon entry and accumulation. At the resident level, regular ventilation practices and targeted public education are essential for reducing exposure. These findings collectively underscore the need for integrated regulatory, environmental, and educational measures to address radon-related health risks in China.

This study has several limitations. Although the 20 cities were selected to represent different regions of China, constraints in research personnel and infrastructure may have limited representativeness. The sample of 1,139 dwellings may not fully capture national indoor radon patterns, and the target of 60 dwellings per city was determined by prior experience and practical considerations rather than formal statistical power calculations. Future studies employing larger, more systematically designed samples are warranted.

doi: 10.46234/ccdcw2026.064

Corresponding authors: Yunyun Wu, wuyunyun@nirp.chinacdc.cn; Xianliang Wang, wangxianliang@nieh.chinacdc.cn.

[1] Key Laboratory of Radiological Protection and Nuclear Emergency, National Institute for Radiological Protection, Chinese Center for Disease Control and Prevention & Chinese Academy of Preventive Medicine, Beijing, China; [2] Key Laboratory of Environment and Population Health, National Institute of Environmental Health, Chinese Center for Disease Control and Prevention & Chinese Academy of Preventive Medicine, Beijing, China.

Submitted: December 31, 2025
Accepted: March 16, 2026
Issued: April 03, 2026

REFERENCES

1. World Health Organization. WHO handbook on indoor radon: a public health perspective. Geneva: World Health Organization. 2009. https://www.who.int/publications/i/item/9789241547673.
2. Darby S, Hill D, Deo H, Auvinen A, Barros-Dios JM, Baysson H, et al.

Residential radon and lung cancer-detailed results of a collaborative analysis of individual data on 7148 persons with lung cancer and 14, 208 persons without lung cancer from 13 epidemiologic studies in Europe. Scand J Work Environ Health 2006;32 Suppl 1:1-83. https://pubmed.ncbi.nlm.nih.gov/16538937/.
3. Krewski D, Lubin JH, Zielinski JM, Alavanja M, Catalan VS, Field RW, et al. Residential radon and risk of lung cancer: a combined analysis of 7 North American case-control studies. Epidemiology 2005;16(2):137 – 45. https://doi.org/10.1097/01.ede.0000152522.80261.e3.
4. Lubin JH, Wang ZY, Boice JD Jr, Xu ZY, Blot WJ, De Wang L, et al. Risk of lung cancer and residential radon in China: pooled results of two studies. Int J Cancer 2004;109(1):132 – 7. https://doi.org/10.1002/ijc.11683.
5. United Nations. Sources and effects of ionizing radiation: United Nations scientific committee on the effects of atomic radiation, UNSCEAR 2000 report to the general assembly, with scientific annexes. New York: United Nations. 2000. https://www.unscear.org/unscear/uploads/documents/unscear-reports/UNSCEAR_2000_Report_Vol.I.pdf.
6. Chen J, Harley NH. A review of indoor and outdoor radon equilibrium factors-part I: 222Rn. Health Phys 2018;115(4):490 – 9. https://doi.org/10.1097/hp.0000000000000909.
7. United Nations. Sources, effects and risks of ionizing radiation: United Nations scientific committee on the effects of atomic radiation, UNSCEAR 2019 report to the general assembly, with scientific annexes. New York: United Nations; 2020. https://www.unscear.org/unscear/uploads/documents/unscear-reports/UNSCEAR_2019_Report-CORR.pdf.
8. Martin-Gisbert L, Kelsey KT, Ruano-Ravina A. Are we underestimating indoor radon exposure in radon priority areas? Occup Environ Med 2025;82(5):213-4. http://dx.doi.org/10.1136/oemed-2025-110093.
9. Zou Y, Lang SW, Xu W, Li Z, Tang YJ, Zhang J, et al. Development and prospects for China's building energy efficiency standards. Build Sci 2016;32(12):1 – 5,12. https://doi.org/10.13614/j.cnki.11-1962/tu.2016.12.01.
10. Ding BW, Wu YY, Song YC, Hou CS, Shang B. Analysis of indoor radon concentration levels and trends in China. Front Public Health 2025;13:1524179. https://doi.org/10.3389/fpubh.2025.1524179.
11. Yao YP, Chen B, Zhuo WH. Reanalysis of residential radon surveys in China from 1980 to 2019. Sci Total Environ 2021;757:143767. https://doi.org/10.1016/j.scitotenv.2020.143767.
12. Arvela H, Holmgren O, Reisbacka H, Vinha J. Review of low-energy construction, air tightness, ventilation strategies and indoor radon: results from Finnish houses and apartments. Radiat Prot Dosimetry 2014;162(3):351 – 63. https://doi.org/10.1093/rpd/nct278.
13. Lembrechts J, Janssen M, Stoop P. Ventilation and radon transport in Dutch dwellings: computer modelling and field measurements. Sci Total Environ 2001;272(1-3):73 – 8. https://doi.org/10.1016/s0048-9697(01)00667-2.
14. McGrath JA, Aghamolaei R, O'Donnell J, Byrne MA. Factors influencing radon concentration during energy retrofitting in domestic buildings: a computational evaluation. Build Environ 2021;194:107712. https://doi.org/10.1016/j.buildenv.2021.107712.
15. Martin-Gisbert L, Ruano-Ravina A, López-Vízcaíno E, Barros-Dios J, Piñeiro-Lamas M, Teijeiro A, et al. The Galician radon map: determining indoor radon exposure through census tracts. Indoor Air 2025;2025(1):4176561. https://doi.org/10.1155/ina/4176561.

Perspectives

The Vector-Proofing Gap in Sponge City Design: Implications for Arboviral Risk Under Climate Adaptation — Guangdong Province, China, 2025

Yu Wang[1]; Xinghai Wu[2]; Bin Xu[3]; Xingui Sun[4]; Zhongjun Guan[5,#]

ABSTRACT

This perspective examines the July 2025 chikungunya fever outbreak in Guangdong Province as a sentinel event exposing a practical gap in climate-resilient urban design. As of July 26, 2025, Guangdong had reported 4,824 confirmed cases, 98.5% in Foshan City and most concentrated in Shunde District. Although sponge-city green stormwater infrastructure (GSI) strengthens urban flood resilience, its detention and retention features can also generate cryptic, hard-to-inspect water habitats that sustain *Aedes* mosquito breeding under hot, humid conditions when post-storm dry-down and maintenance fall short. This perspective synthesizes outbreak context, China's sponge-city evaluation metrics, and vector-ecology thresholds to define a vector-proofing gap: prevailing sponge-city guidance excels in hydrological performance but typically lacks explicit, measurable constraints on water residence time and inspectability tied directly to vector risk. An operational vector-proofing framework is proposed that 1) translates entomological risk into engineering indicators (e.g., post-storm dry-down within 48–72 hours where feasible, access/inspectability, and trigger-based maintenance), 2) embeds vector impact assessment across the project lifecycle, and 3) clarifies cross-sector responsibilities among housing/urban–rural development, water resources, and health agencies. Aligning hydrological and entomological objectives can reduce the likelihood that climate adaptation investments inadvertently shift risk from flooding to arboviral transmission.

On July 9, 2025, Foshan City in Guangdong Province reported a cluster of chikungunya fever cases. By July 26, the provincial total had reached 4,824 confirmed cases across 12 prefecture-level cities: 4,754 (98.5%) in Foshan and 4,208 (87.2% of the provincial total) heavily concentrated in Shunde District (*1*). Notably, Shunde has also served as a core area for the high-density implementation of sponge-city green stormwater infrastructure (GSI) in recent years, producing a striking spatial overlap between the outbreak epicenter and GSI proliferation.

In Guangdong, *Ae. albopictus* predominates as the primary mosquito vector, whereas *Ae. aegypti* has a comparatively limited distribution — an ecological context that shapes outbreak dynamics and control options. Genomic surveillance confirmed that the circulating strain belongs to the Middle African Lineage (MAL) within the East/Central/South African (ECSA) genotype and carries adaptive mutations including E1-A226V, E2-L210Q, and E2-I211T, which enhance viral replication and transmission efficiency specifically in *Ae. albopictus* (*2*).

Concurrently, Guangdong's rapidly urbanizing cities have expanded sponge-city GSI — including permeable pavements, bioretention basins, rain gardens, and constructed wetlands — to detain runoff and buffer extreme rainfall. These systems are central to climate adaptation yet inevitably alter urban micro-ecologies and hydrological cycles. This ecological side effect constitutes a form of adaptive risk transfer: infrastructure optimized for flood mitigation may impose downstream burdens on vector surveillance and infectious disease prevention when biological safety is not explicitly built into design and maintenance. Accordingly, this perspective frames a climate adaptation paradox as a testable maladaptation pathway — infrastructure designed to mitigate flooding may, under hot–wet extremes and operational constraints, elevate *Aedes*-borne risk. This perspective does not claim that sponge-city facilities caused the 2025 outbreak; rather, it clarifies a plausible mechanism and proposes measurable "vector-proofing" indicators and governance pathways for integrating vector risk into sponge-city design, acceptance, and maintenance (*3*).

Approach and Evidence Base

The evidence base integrates: 1) two China CDC Weekly reports on the 2025 Guangdong chikungunya outbreak and its virologic context (*1*–*2*); 2) China's national sponge-city evaluation standard (GB/T 51345-2018), which characterizes prevailing hydrology-centered performance metrics (*3*); and 3) public-health guidance and peer-reviewed evidence on mosquito-breeding thresholds in stormwater control structures and temperature-dependent development (*4*–*5*). The Foshan outbreak report also documented real-time vector surveillance using the Breteau Index and Area Density Index, with control measures deployed within a 100 m radius of case locations; this provides local outbreak and entomological context but does not constitute facility-level evidence on GSI types, standing-water duration, maintenance status, or larval productivity around specific sponge-city assets. Where such Guangdong-specific facility-level measurements are unavailable in the reviewed sources, we explicitly distinguish inference from evidence and treat the proposed mechanism as a plausible, testable hypothesis rather than a demonstrated causal pathway.

Accordingly, this manuscript does not attempt causal attribution, employ control-area comparisons, or present facility-level surveillance data; instead, it synthesizes outbreak context, standards, and vector-ecology evidence to define a testable, policy-relevant hypothesis. China's national *Aedes* surveillance practice already uses larval and ovitrap indicators for risk warning and response stratification, demonstrating that surveillance-linked maintenance is operationally feasible in Chinese settings (*6*).

The Adaptation Paradox: Hydrology *vs.* Entomology

Sponge-city GSI is typically optimized for hydrological performance — encompassing runoff volume control, detention/retention capacity, water quality improvement, and urban heat-island co-benefits — as reflected in China's national evaluation standard GB/T 51345-2018 (*3*). Although this standard meticulously evaluates macroscopic hydrological indicators such as the Runoff Volume Control Ratio and Total Suspended Solids (TSS) removal, it omits biological safety indicators pertaining to disease vectors or pathogen transmission. In practice, hydrology-centered metrics rarely translate vector safety into explicit, measurable constraints on post-storm dry-down time, inspectability, or surveillance-linked maintenance triggers. The resulting gap between prevailing hydrology-centered performance metrics and measurable vector-safety indicators is summarized in Table 1.

The core tension centers on water residence time: detention and retention improve runoff management, yet persistent surface or cryptic water can sustain *Aedes* immature development and amplify local vector capacity. Operationally, risk remains low when surface ponding drains rapidly — for example, within 24 hours — but escalates when ponding persists beyond 48–72 hours or when subsurface voids create inaccessible water pockets. Field performance can deviate from design specifications because of clogged underdrains, soil compaction, subsidence, or organic debris, leaving small but stable water volumes in bioretention cells, permeable pavement bases, vegetated swales, or curb inlets. These observations motivate vector-proofing: residence time and inspectability

TABLE 1. The vector-proofing gap: hydrology-centered metrics versus measurable vector-safety metrics.

Current focus	Vector-proofing metrics	Operational hook
Runoff volume control, detention/retention capacity targets	Post-storm dry-down time (e.g., ≤48–72 h where feasible for surface ponding)	Standing-water duration audits after representative storms; design drain-down capacity; maintenance triggers when exceedance observed
Water quality/pollutant settling	Avoid persistent shallow stagnant water; manage sediments and margins to reduce oviposition habitats	Sediment removal schedule; margin management; documented post-storm inspections for blocked outlets/underdrains
Ecological greening/vegetation coverage	Vegetation structure that avoids dense shaded cryptic pools and trapped water	Routine pruning and litter removal; avoid vegetation that traps water; recordable checklist items
Lifecycle delivery emphasizes design and construction	Inspectability and access (ability to find and treat cryptic habitats)	Access ports/cleanouts; standardized inspection points; asset register linking each facility to O&M responsibility
Flood-risk governance and O&M not linked to public health metrics	Vector indices linked to O&M (e.g., BI/ovitrap/adult trap thresholds near GSI)	Surveillance results trigger work orders; joint dashboards between city maintenance and CDC/health agencies

Abbreviation: h=hour; O&M=operation and maintenance; BI=breteau index; GSI=green stormwater infrastructure.

should function as primary performance criteria alongside hydrological targets. As a practical rule of thumb, stormwater control structures should hold water for fewer than 72 hours whenever possible, so that retention time remains shorter than the minimum period generally required for immature mosquito development to reach emergence (*4*). For *Ae. albopictus*, laboratory evidence indicates that immature development is shortest at approximately 30 ℃, averaging about 8.8 days, suggesting that warmer urban microclimates can further compress development time (*5*). Accordingly, a conservative operational target is post-storm dry-down within 48–72 hours where feasible for surface ponding. Where longer retention is required, such as in permanent pools or inaccessible subsurface structures, designs should prevent oviposition, remain inspectable, and include explicit access points and maintenance protocols. These thresholds are species- and temperature-dependent and should therefore be calibrated to local vector ecology and seasonal conditions.

Mechanisms of Risk in Urban GSI

In hot, humid subtropical cities, sponge-city GSI creates a highly distributed network of small water-holding structures embedded within residential streetscapes and public spaces. This decentralization complicates conventional vector control, which is often optimized for identifiable container habitats or centralized drainage assets. During intense rainfall periods — including Guangdong's typhoon season — repeated storm events and short inter-event dry periods magnify the operational importance of rapid drain-down, debris removal, and routine inspection across numerous dispersed sites.

First, cryptic habitats matter: small water volumes trapped in curb inlets, underdrains, or subsurface voids of permeable pavements can be visually undetectable and difficult to treat, enabling oviposition and larval survival beyond the reach of routine larviciding. Empirical evidence from urban China supports the plausibility of drainage-associated mosquito production — in downtown Shanghai, *Ae. albopictus* breeding was documented in stormwater catch basins and manhole chambers, demonstrating that concealed water-holding structures in dense cities can function as productive larval habitats (*7*). Second, microclimate accelerates development: urban heat shortens immature development and gonotrophic cycles; for *Ae. albopictus*, immature development averages approximately 8.8 days at approximately 30 °C (*5*). Third, vegetation can increase adult survival by providing shaded, humid resting sites that potentially raise local biting pressure. Together, these mechanisms motivate measurable controls — dry-down targets, access points, and surveillance-triggered maintenance — rather than reliance on hydrology-only performance criteria. As Figure 1 illustrates, the convergence of cryptic habitats, climate extremes, and vegetation structure creates a feedback loop that amplifies vector capacity.

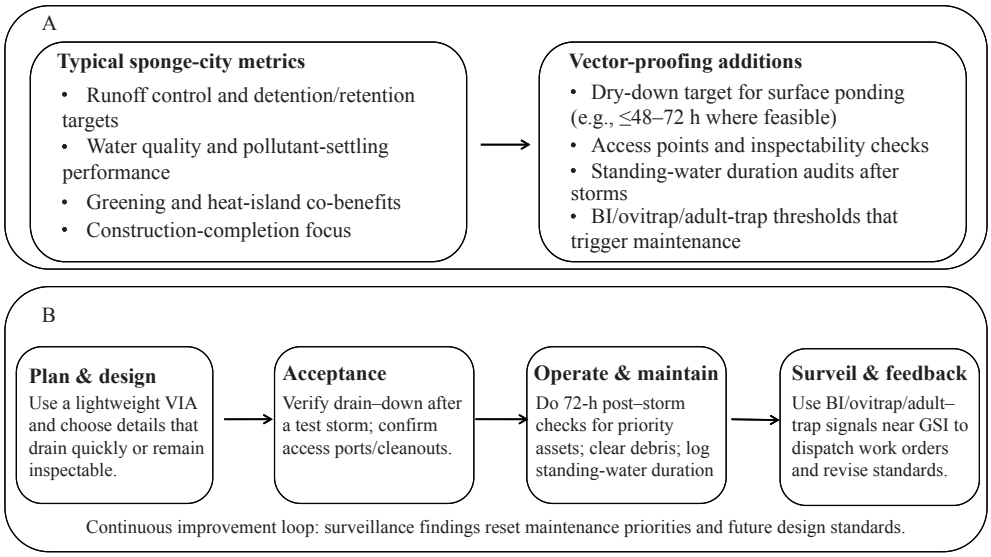

FIGURE 1. Operational vector-proofing framework for sponge-city infrastructure, Guangdong Province, China, 2025. (A) Metrics gap: hydrology targets → vector-safe operating targets; (B) Implementation loop: embed indicators across the asset lifecycle.

Policy Implications for Healthy China

This Perspective does not argue against sponge-city development; rather, it emphasizes the need to align climate-resilience investments with infectious disease prevention. The 2025 Guangdong outbreak illustrates that biological risk can emerge from routine infrastructure when residence time and inspectability are not actively managed (*1*–*2*). This rationale aligns with the China National Climate Change Health Adaptation Action Plan (2024–2030), which calls for interdepartmental coordination, surveillance capacity, and adaptation measures that explicitly address climate-sensitive health risks (*8*). Existing *Aedes* surveillance practice in China further demonstrates that entomological indicators can be linked to operational thresholds for maintenance and rapid response (*6*). Closing this gap requires an explicit implementation pathway: entomological indicators must be translated into engineering specifications and embedded at each lifecycle stage — planning and design, construction acceptance, and routine operation and maintenance. The division of responsibilities must be clearly delineated: housing and urban–rural development authorities should update civil engineering codes to mandate inspectability and physical barriers; water resources and municipal maintenance departments should execute routine clearing and audit standing-water duration; and health agencies (NHC and CDCs) should define entomological thresholds and conduct Vector Impact Assessments (VIA) prior to construction. This staged approach is also consistent with integrated vector-management principles emphasizing surveillance-based decision-making, intersectoral coordination, and adaptive operations across sectors (*9*).

Recommendations

To reconcile flood management with disease prevention, vector-proofing should be implemented as a staged package with explicit lead bodies, cost/complexity benchmarks, and timelines (Table 2). A conservative target of post-storm dry-down within 48–72 hours should be pursued where feasible for surface ponding, while high-risk structures unable to meet this target should require sealed design, inspectability, and additional vector-control measures. However, given Guangdong's subtropical climate and heavy typhoon-season rainfall, gravity-driven soil infiltration alone may be insufficient in some high-risk settings; consequently, secondary interventions — such as completely sealed catch basin covers or embedded slow-release biological larvicides (e.g., *Bacillus thuringiensis israelensis*) — should be considered or may be required for selected high-risk drainage infrastructure (*10*). This target serves as an operational risk-reduction benchmark rather than a universal compliance threshold and should be adapted to local rainfall regimes, asset function, and the distinction between surface ponding and subsurface retained water.

CONCLUSION

The 2025 Guangdong chikungunya outbreak — concentrated in Foshan City and Shunde District — underscores that climate adaptation infrastructure can create unintended arboviral risk when water residence time and inspectability are not operationalized (*1*). Vector-proofing offers a pragmatic extension of sponge-city practice: it introduces measurable dry-down and access indicators, links routine surveillance to maintenance dispatch, and clarifies cross-sector roles throughout planning, acceptance, and operation. Implementing these steps can reduce the likelihood that flood-resilience investments inadvertently shift risk toward *Aedes*-borne transmission, while generating the

TABLE 2. Implementation Roadmap for Vector-Proofing of Sponge-City Infrastructure.

Priority	Action	Lead bodies	Cost	Timeline
NOW	Sentinel GSI surveillance; BI/ovitrap/adult thresholds trigger work orders.	Municipal CDC + city maintenance	Low–Mod	0–6 months
NOW	72-h post-storm checks for priority assets; clear debris; log standing-water duration.	Maintenance contractors + water bureau	Low	0–6 months
NEXT	Design/acceptance checklist: verify drain-down, eliminate cryptic pooling, require access ports.	Housing/urban bureau + water + CDC	Mod	6–18 months
NEXT	Lightweight Vector Impact Assessment (VIA) for new or retrofitted GSI in high-risk districts.	Planning + housing/urban + CDC	Mod	6–18 months
LATER	Revise local standards and procurement to add dry-down, inspectability, and trigger metrics; build a shared risk dashboard.	Provincial/municipal standard bodies + NHC/CDC	High	18–36 months

Abbreviation: GSI=Green Stormwater Infrastructure; BI=Breteau Index; Mod=Moderate; h=hour; VIA=Vector Impact Assessment; NHC=National Health Commission.

facility-level evidence needed to test and refine the proposed mechanism.

Conflicts of interest: No conflicts of interest.

Acknowledgments: The National Health Talent Capacity Building Project of the Institute of Public Welfare and Philanthropy — the Elite Empowerment Program for Building a Healthy China (2025) — for its support.

Funding: Supported by Capital's Funds for Health Improvement and Research (2024-1G-2013).

doi: 10.46234/ccdcw2026.068

[#] Corresponding author: Zhongjun Guan, guanzhj@ccmu.edu.cn.

[1] School of Public Health, Peking University, Beijing, China; [2] Chuiyangliu Hospital Affiliated with Tsinghua University, Beijing, China; [3] Beijing Tiantan Hospital, Capital Medical University, Beijing, China; [4] Beijing Center for Disease Prevention and Control, Beijing, China; [5] Xuanwu Hospital, Capital Medical University, Beijing, China.

Submitted: December 29, 2025
Accepted: March 20, 2026
Issued: April 03, 2026

REFERENCES

1. Li YH, Jiang SY, Zhang M, Li Y, He JF, Yang ZF, et al. An outbreak of chikungunya fever in China — Foshan City, Guangdong Province, China, July 2025. China CDC Wkly 2025;7(32):1064 – 5. https://doi.org/10.46234/ccdcw2025.172.
2. Gong WX, Wang DL, Chen QY, Zhong ST, Shi XL, Peng B. Outbreak of chikungunya virus with *Aedes albopictus*-adaptive mutations — Guangdong Province, China, 2025. China CDC Wkly 2025;7(49): 1528 – 32. https://doi.org/10.46234/ccdcw2025.260.
3. Ministry of Housing and Urban-Rural Development of the People's Republic of China. GB/T 51345-2018 Assessment standard for sponge city construction effect. Beijing: China Architecture & Building Press, 2018. http://www.csres.com/detail/326369.html. (In Chinese).
4. National Center for Environmental Health (U.S.), Division of Emergency and Environmental Health Services. Stormwater management and vector breeding habitats. Atlanta: CDC; 2012. https://stacks.cdc.gov/view/cdc/48388.
5. Delatte H, Gimonneau G, Triboire A, Fontenille D. Influence of temperature on immature development, survival, longevity, fecundity, and gonotrophic cycles of *Aedes albopictus*, vector of chikungunya and dengue in the Indian Ocean. J Med Entomol 2009;46(1):33 – 41. https://doi.org/10.1603/033.046.0105.
6. Liu XB, Liu QY. Aedes surveillance and risk warnings for dengue — China, 2016-2019. China CDC Wkly 2020;2(24):431 – 7. https://doi.org/10.46234/ccdcw2020.111.
7. Gao Q, Wang F, Lv XH, Cao H, Su F, Zhou JJ, et al. *Aedes albopictus* production in urban stormwater catch basins and manhole chambers of downtown Shanghai, China. PLoS One 2018;13(8):e0201607. https://doi.org/10.1371/journal.pone.0201607.
8. Shi XM, Wang L, Dai Z, Xu DQ, Ban J, Pan LJ, Tang XZ. Policy interpretation of the China national climate change health adaptation action Plan (2024-2030). China CDC Wkly 2025;7(12):385 – 8. https://doi.org/10.46234/ccdcw2025.063.
9. World Health Organization. Global vector control response 2017-2030. Geneva: World Health Organization; 2017. https://www.who.int/publications/i/item/9789241512978.
10. Anderson JF, Ferrandino FJ, Dingman DW, Main AJ, Andreadis TG, Becnel JJ. Control of mosquitoes in catch basins in Connecticut with *Bacillus thuringiensis israelensis, Bacillus sphaericus*, and spinosad. J Am Mosq Control Assoc 2011;27(1):45 – 55. https://doi.org/10.2987/10-6079.1.

Youth Editorial Board

Indexed by Science Citation Index Expanded (SCIE), Social Sciences Citation Index (SSCI), PubMed Central (PMC), Scopus, Chinese Scientific and Technical Papers and Citations, and Chinese Science Citation Database (CSCD)

The inauguration of *China CDC Weekly* is in part supported by Project for Enhancing International Impact of China STM Journals Category D (PIIJ2-D-04-(2018)) of China Association for Science and Technology (CAST).

CHINA CDC WEEKLY

CCDC weekly

Vol. 8 No. 14 Apr. 3, 2026

中国疾病预防控制中心周报(英文)

Responsible Authority
National Disease Control and Prevention Administration

Sponsor
Chinese Center for Disease Control and Prevention

Editor-in-Chief
Jianwei Wang

Editing and Publishing
China CDC Weekly Editorial Office
No.155 Changbai Road, Changping District, Beijing, China
Tel: 86-10-63150501, 63150701
Email: weekly@chinacdc.cn

Printing: Beijing Kexin Printing Co., Ltd

Complimentary Access

CSSN
ISSN 2096-7071 (Print)
ISSN 2097-3101 (Online)
CN 10-1629/R1